PAPER • OPEN ACCESS

Sensitivity analysis of effective transverse shear viscoelastic and diffusional properties of myelinated white matter

View the article online for updates and enhancements.

Physics in Medicine & Biology

IPEM Institute of Physics and Engineering in Medicine

CrossMark

PAPER

Sensitivity analysis of effective transverse shear viscoelastic and diffusional properties of myelinated white matter

Daniel J Sullivan[1] , Xuehai Wu[1], Nicolas R Gallo[2], Noel M Naughton[3] , John G Georgiadis[2,3] and Assimina A Pelegri[1,*]

[1] Department of Mechanical and Aerospace Engineering, Rutgers, the State University of New Jersey, 98 Brett Road, Piscataway, NJ 08854-8058, United States of America
[2] Department of Biomedical Engineering, Illinois Institute of Technology, 3255 S. Dearborn St., Wishnick Hall 314, Chicago, IL 60616, United States of America
[3] Department of Mechanical Science and Engineering, University of Illinois at Urbana–Champaign, 1206 W Green St., Urbana, IL 61801, United States of America
[*] Author to whom any correspondence should be addressed.

E-mail: pelegri@rutgers.edu

Abstract

Motivated by the need to interpret the results from a combined use of *in vivo* brain Magnetic Resonance Elastography (MRE) and Diffusion Tensor Imaging (DTI), we developed a computational framework to study the sensitivity of single-frequency MRE and DTI metrics to white matter microstructure and cell-level mechanical and diffusional properties. White matter was modeled as a triphasic unidirectional composite, consisting of parallel cylindrical inclusions (axons) surrounded by sheaths (myelin), and embedded in a matrix (glial cells plus extracellular matrix). Only 2D mechanics and diffusion in the transverse plane (perpendicular to the axon direction) was considered, and homogenized (effective) properties were derived for a periodic domain containing a single axon. The numerical solutions of the MRE problem were performed with ABAQUS and by employing a sophisticated boundary-conforming grid generation scheme. Based on the linear viscoelastic response to harmonic shear excitation and steady-state diffusion in the transverse plane, a systematic sensitivity analysis of MRE metrics (effective transverse shear storage and loss moduli) and DTI metric (effective radial diffusivity) was performed for a wide range of microstructural and intrinsic (phase-based) physical properties. The microstructural properties considered were fiber volume fraction, and the myelin sheath/axon diameter ratio. The MRE and DTI metrics are very sensitive to the fiber volume fraction, and the intrinsic viscoelastic moduli of the glial phase. The MRE metrics are nonlinear functions of the fiber volume fraction, but the effective diffusion coefficient varies linearly with it. Finally, the transverse metrics of both MRE and DTI are insensitive to the axon diameter in steady state. Our results are consistent with the limited anisotropic MRE and co-registered DTI measurements, mainly in the *corpus callosum*, available in the literature. We conclude that isotropic MRE and DTI constitutive models are good approximations for myelinated white matter in the transverse plane. The unidirectional composite model presented here is used for the first time to model harmonic shear stress under MRE-relevant frequency on the cell level. This model can be extended to 3D in order to inform the solution of the inverse problem in MRE, establish the biological basis of MRE metrics, and integrate MRE/DTI with other modalities towards increasing the specificity of neuroimaging.

1. Introduction

Constituting approximately 50% of the brain and 60%–80% of the spinal cord in humans, white matter (WM) is highly significant in disease or senescence (Saab and Nave 2017, Fern 2017). Loss in WM integrity is

a core feature of multiple sclerosis, traumatic brain injury, and vascular dementia. Brain imaging indicates that damages in myelinated axons precede most neurodegenerative diseases like Alzheimer's (Dean *et al* 2017), amyotrophic lateral sclerosis (Foerster *et al* 2013), Huntington's (Gatto *et al* 2015) and Parkinson's (Duncan *et al* 2016) diseases, and are correlated with age-related declining performance on cognitive or motor tests (Sullivan *et al* 2010). Beyond Diffusion Tensor Imaging (DTI), significant progress has been made in diffusion-weighted MRI (dMRI) (Le Bihan and Johansen-Berg 2012), but dMRI metrics alone are not specific to these WM changes. The interpretation of dMRI signal is often confounded by additional changes, such as axonal degeneration or inflammatory cell infiltration (Song *et al* 2005, Sun *et al* 2006, Wang *et al* 2011), or mechanical injury and recovery of axons in traumatic brain injury (Eierud *et al* 2014). Therefore, novel adjunctive MRI modalities are sought towards increasing the biological basis and specificity of brain imaging.

One such promising modality is Magnetic Resonance Elastography (MRE) (Muthupillai *et al* 1995), which enables the extraction of local mechanical properties by interpreting the propagation of harmonic shear waves in tissue created by external excitation at 20–100 Hz (for the human brain). The MRE methodology involves displacement data acquisition to encode the resulting shear deformation in the tissue, followed by the computational solution of an inverse problem to extract the local mechanical properties of the tissue from the displacement field. While highlighting the dramatic progress made during the last 20 years, a recent review of brain MRE (Murphy *et al* 2019) concludes with a suggestion that there are two areas that require immediate attention: further improvement of resolution and more investigation into the biological basis of stiffness (and of MRE metrics, by extension). *In order to address these needs systematically, we propose to revisit the micromechanics of the WM that are relevant to MRE.* The justification is based on a number of arguments. First, we posit that improvements in MRE resolution hinge on better acquisition strategies in conjunction with inversion of the appropriate model, with the latter intimately connected with a representative material (mechanical) model embodying an appropriate stress-strain relationship (constitutive law). Solely improving the accuracy of the inversion algorithm cannot offset any mechanical model deficiencies; the extracted MRE metrics would depend on the actuation procedure or inversion method rather than reflecting the underlying physics. Second, we suggest that adopting an accurate tissue-based model constitutes a rational first step towards the interpretation of MRE metrics (e.g. viscoelastic moduli) in terms of tissue microarchitecture and intrinsic properties of its constituent cells, which are intimately connected to both normal or pathological processes. Third, establishing appropriate tissue-based models allows the systematic integration of MRE with other adjunctive MR modalities, such as dMRI, in order to improve MRE for neuroimaging.

Both MRE and dMRI metrics reflect voxel-averaged (effective) properties and rely on tissue (sub-voxel) models to account for the microstructure and intrinsic properties of the components (cell constituents) in each voxel. The interpretation of dMRI signal is based on multiphase models of water diffusion in the brain representing the various signal 'pools', with a concomitant improvement of the ability of the underlying tissue models to distinguish between the axon and glial contributions to the signal (Stanisz *et al* 1997, Sen and Basser 2005, Assaf and Basser 2005, Hall and Alexander 2009, Panagiotaki *et al* 2012, Kaden *et al* 2016, Kiselev 2017, Jelescu and Budde 2017, Veraart *et al* 2019). There is a plethora of dMRI metrics, each based on a different biophysical WM model, for example, DTI, DKI (Diffusional Kurtosis Imaging), NODDI (Neurite Orientation Dispersion and Density Imaging), WMTI (White Matter Track Integrity), etc (Jelescu and Budde 2017). For definitiveness, we will focus here on DTI metrics that are combinations of the diffusion tensor eigenvalues, which are the effective diffusion coefficients (averaged over the voxel). In contrast, the majority of prior brain MRE studies reviewed in (Murphy *et al* 2019) are based on *a priori* constitutive models of the brain, which represent the whole brain as a linear viscoelastic and isotropic material. Unlike DTI, the isotropic MRE material model returns a single property pair (stiffness or storage modulus, $G\prime$, and loss modulus, $G\prime\prime$,) that is some composite of direction-dependent shear moduli, and thus is inadequate for separating contributions to tissue stiffness from axons and glia, or from their interface. WM is known to be mechanically anisotropic under shear on the millimeter scale, especially in regions with high directional coherence, such as the *corpus callosum* and *corona radiata* (Velardi *et al* 2006, Feng *et al* 2013). The need to choose the correct mechanical problem to invert has become more urgent as both the spatial resolution and accuracy of *in vivo* brain MRE has improved, first achieving 2 mm (McGarry *et al* 2012, 2013, Johnson *et al* 2013a, 2013b) and then 1.6 mm isotropic voxels (Johnson *et al* 2014). By separately exciting the brain in two different directions, the consequences of the mechanical anisotropy of WM on MRE metrics have been shown to be very important (Anderson *et al* 2016). Isotropic inversions of the two separate displacement fields resulted in mechanical property maps that are disparate between the excitations in regions of highly aligned WM. Specifically, reconstruction of G' and G'' in the *corpus callosum, corona radiata*, and *superior longitudinal* fasciculus revealed property differences between excitations of up to 33%.

An early attempt to incorporate more tissue microstructure in an isotropic brain model was based on a 2-parameter 'springpot' viscoelastic model (Posnansky *et al* 2012, Guo *et al* 2012), inspired by a ladder model of tissue as a fractal network (Schiessel and Blumen 1995). The effective properties lack specificity and are only an indirect characterization of the microstructure. Prior anisotropic MRE studies have relied on the assumption that WM tissue is represented by transversely isotropic (Sinkus *et al* 2005a, Papazoglou *et al* 2006, Qin *et al* 2013, Schmidt *et al* 2016, 2018) or orthotropic (Romano *et al* 2012, 2014) constitutive laws parameterized by a few mechanical parameters. Although entirely plausible, these models are not derived based on the tissue microstructure. Anisotropic models have been utilized to correlate the MRE metrics with normal brain aging (Kalra *et al* 2019, Gallo *et al* 2019) and certain pathologies, e.g. amyotrophic lateral sclerosis (Romano *et al* 2014), but their *a priori* nature does not allow the separation of the effect of the microstructure from the intrinsic properties of the constituents (axons, myelin, glial cells). As the growing body of *in vivo* brain MRE studies demonstrate (Murphy *et al* 2019), there is a correlation between tissue stiffness decreases with normal aging or level of dementia, but these changes cannot be assigned to specific microstructural events. Without this assignment, MRE cannot differentiate between the different pathologies coexisting in the aging brain, as well as separate the confounding effects of edema, inflammation, or intracranial pressure variation. Unless the model accommodates changes in neuro-architecture and intrinsic tissue properties separately, the investigator has to merely rely on correlations between MRE metrics and putative pathophysiology. More importantly, information from other *ex vivo* and *in vivo* studies cannot be exploited optimally to design the next MRE study. For example, it is not known how the model should be formulated rationally to account for the reduction in the number of myelinated axons, alterations in fiber diameter, degenerative changes to the myelin sheath, as well as remyelination associated with normal aging (Morrison and Hof 1997). It is not known how these structural changes should be used systematically to interpret prior -or inform future- human MRE studies because the sensitivity of the derived MRE metrics to these changes is not known.

The integration of MRE and DTI has been already advocated based on progress in breast elastography (Sinkus *et al* 2005a, 2005b). Specifically, Sinkus and collaborators have proposed a transversely isotropic mechanical model for soft fibrous tissue MRE based on local fiber orientation extracted from DTI, which was validated on simple anisotropic viscoelastic phantoms and bovine muscle samples (Qin *et al* 2013). However, the proposed inversion method relies on assuming that mechanical properties vary slowly in space, which is not justified in the case of brain WM. Recently, the classical dMRI metrics (Jelescu and Budde 2017) are supplemented by additional dMRI metrics that are more sensitive to WM microstructure changes during healthy aging (Branzoli *et al* 2016, Guerreri *et al* 2019). In addition, there are alternate MRI modalities that can complement MRE by probing specific WM microstructural features *in vivo* (Stikov *et al* 2015, Björnholm *et al* 2017, Berman *et al* 2018, West *et al* 2018). These extra modalities provide information about specific cellular compartments (intracellular diffusion, myelin volume fraction, ratio of myelin to axon size), but similarly to DTI, both sequence design and signal interpretation depend on assumed microstructure models and associated spin kinetics.

Rather than starting from an *a priori* constitutive model, we focus here on developing a WM tissue model starting from the microstructure. The dual challenge is to capture all the relevant physics that impact the voxel-averaged MRE signal, while the model remains parsimonious. Using a minimal model to interpret the measurements ultimately results in a tractable inverse problem. Our approach is to start with a large set of topological and material parameters that are relevant to the response of the tissue under the MRI protocols, and then eliminate those parameters that do not significantly affect the measurements. MRE and DTI measure the effective mechanical and diffusive properties of brain parenchyma, so a systematic approach to meet the challenge is to model the underlying micromechanics and diffusion physics at scales that are relevant to the imaging physics. Typical MRE and DTI pulse sequences render the MRI signal sensitive to proton spin displacements on the micrometer scale; the first encoding coherent (harmonic), while the second incoherent displacements. On the other hand, both clinical (*in vivo*) MRE and DTI have a practical voxel resolution limit of ~ 1 millimeter. All structural information below this spatial scale is 'smeared' but not lost. An established method to recover microstructural information is based on exploiting the organization of WM microstructure and the underlying physics. In analogy with biophysical DTI models (Fieremans and Lee 2018), a candidate micromechanical model of WM involves a unidirectional composite with axonal fibers embedded in a glial matrix. This is a canonical topology that corresponds to realistic cyto-architectures, and which can be related to WM micrographs extracted through brain sectioning and microscopy (Lee *et al* 2019). We propose modeling the physics of both MRE and DTI on the same tissue model at the microscale. The justification for pursuing an integrated MRE-DTI tissue model is two-fold: First, DTI provides the local orientation of the axons that allows the proper alignment of the micromechanical tissue in the WM. Second, it is conceivable that using both DTI and MRE (effective) metrics, the local intrinsic (phase-specific) properties can be extracted by the established relationship

between effective and intrinsic properties. There is no coupling between MRE and DTI physics, only additional information that can be used to estimate the properties of each cellular phase.

At this point, it is important to contrast the constraints of MRE with those of other *ex vivo* mechanical characterization methods for brain tissue. *In vivo* brain MRE is based on low frequency (50 Hz), micron-size displacements and low shear strain ($\sim 10^{-4}$) harmonic excitation and detection of the shear waves. *Ex vivo* methods involve medium to large strains under quasistatic, creep/relaxation, constant strain tensile/compression, oscillatory shear, indentation, or impulsive actuation of brain tissue (Chatelin *et al* 2010). The large scatter of data reported in (Chatelin *et al* 2010) exemplifies the fact that the effective brain tissue properties depend strongly on the loading conditions, as well as test conditions (Hrapko *et al* 2008). Recent shear elastography studies have revealed the significant effect of varying intracranial pressure (Arani *et al* 2017, Tzschätzsch *et al* 2018) and temperature (Liu *et al* 2017), as well as the resulting tissue alterations during the excision procedure (Guertler *et al* 2018, Liu *et al* 2018). The development of a microstructural model that can accommodate the effects of different loading and test conditions will allow the incorporation of *ex vivo* studies to interpret or validate *in vivo* brain MRE studies. Inspired by the established body of knowledge on the mechanics of composites (Christensen 2005), there are a number of micromechanical studies (Abolfathi *et al* 2009, Pan *et al* 2011, Giordano and Kleiven 2014, Yousefsani *et al* 2018, Recchia *et al* 2014, Pan *et al* 2013, Zhao and Pelegri 2014a, 2014b, 2016, Wu *et al* 2019, Pan *et al* 2020) that describe fibrous material structures and soft fibrous tissue response to many of the above loads (including their combinations) other than the actuation pertinent to brain MRE. A biphasic (glia-axon) fiber-reinforced composite model was employed by (Arbogast and Margulies 1999) to interpret the harmonic viscoelastic response of the brain stem. There is no published study (to our knowledge) of micromechanical models of WM tissue as a triphasic (glia-myelin-axon) composite under harmonic shear. Moreover, there are no systematic sensitivity analyses of WM effective mechanical properties by varying all intrinsic (phase-specific) parameters involved.

The present study addresses the following aims:

- Develop an integrated WM tissue model to extract effective metrics for MRE and DTI, based on rational mechanics and diffusion physics, respectively. Our focus remains on multiphasic biophysical models based on WM cell-level microstructure contained in a tissue-based representative elemental volume (REV). Given the lack of prior work with triphasic models, it is reasonable to start with a 2D homogenization model involving only physics in the plane perpendicular to the axons.
- Perform a sensitivity analysis to determine which intrinsic (microstructural and phasic) parameters are important to the theoretical REV-averaged effective MRE and DTI metrics, both obtained from steady-state simulations. These metrics are computed in the same REV (representing a co-registered MRE/DTI voxel) directly from the underlying physics, rather than for specific MRE or DTI sequences.
- Discuss the limitations of the WM tissue model, reduction of model parameters, potential applications in interpreting MRE/DTI experiments, and possible extensions of the WM model and sensitivity analysis.

The overarching aim of the present study is to establish a systematic framework capable of integrating MRE and DTI into an analytical -not merely descriptive- method of probing the brain WM in health or disease.

2. Materials & methods

2.1. White matter tissue biophysical model

Building upon our prior systematic work on axon-glial interaction models built from experiments with chicken embryos (Pan *et al* 2011), we focus here on the development of an MRE-relevant model of brain WM starting with the interactions between single axons and glial cells. We consider the geometry and mechanical properties of three compartments: axons, glial phase, and myelin. Rather than simply serving as 'glue' to the associated axons, glial cells (oligodendrocytes, neurolemmocytes, and astrocytes) maintain multifunctional and bidirectional interactions with axons throughout life (Saab and Nave 2017). The glial phase consists of these glial cells and a much softer extracellular matrix (glycosaminoglycans, proteoglycans, etc) (Ruoslahti 1996). Henceforth, we will use 'glia' to refer to the glial phase as a whole. The axon cytoskeleton contains longitudinally aligned microtubules (nanoscale structures), which are highly cross-linked in the transverse plane (De Rooij *et al* 2017), *so we can assume that individual axons are mechanically isotropic in the plane perpendicular to their axis.* (Recall that both MRE and DTI are sensitive to the micrometer length scale, which is comparable to cell size, but imaging resolution is ~ mm.) Oligodendrocytes can connect as many as 50 segments of different axons through myelin sheaths, but their spatial organization, as well as that of the other glial cells, is not ordered on the micrometer scale. A

theoretical study of dynamic shear response of 2D cross-linked random fiber networks revealed that, at the limit of long wavelengths, the mechanics are controlled by the elastic properties of the constituents and not by the network connectivity (Babaee *et al* 2015). Indeed, brain MRE involves shear wavelengths of the order of cm (Johnson *et al* 2013a), which is much larger than the distance between individual axons. Consequently *we propose that the glial matrix in 2D can be considered as an isotropic continuum with uniform viscoelastic moduli.* Finally, the myelin sheath around each individual axon exhibits a compact periodic nanostructure, and we similarly *consider it as an isotropic uniform phase.* Consequently, the WM is represented by a unidirectional composite, and each representative elementary volume (REV) contains the cross-section of a single cylindrical axon with the surrounding myelin annulus, immersed in glial matrix, cf figure 1(b). Furthermore, the three phases, axon, myelin and glia, are all *perfectly bonded.* This system is excited by imposing harmonic shear stress at two opposite boundaries of the REV, in a spatially periodic manner, and at a single frequency (50 Hz) that is typically used for *in vivo* brain MRE.

Each phase is assigned isotropic mechanical and diffusional properties, which are piece-wise uniform. An assessment of the intrinsic properties of the components of this composite reveals that (a) axons restrict water diffusion (Beaulieu 2009), and (b) stiffness and viscosity increase as glial matrix < composite < myelinated axon (Lu *et al* 2006, Abolfathi *et al* 2009, Shreiber *et al* 2009). Practical ranges for the viscoelastic properties were developed based on ex-vivo data. A lower bound of intrinsic properties for the glial cells was derived from scanning force microscopy data for hippocampal glial cells (Lu *et al* 2006). Data was interpolated using a power law relationship as a function of frequency, obtaining $G'_{glia} = 116$ Pa and $G''_{glia} = 51.1$ Pa at 50 Hz. Reference values for axons were derived from porcine brainstem data obtained by (Arbogast and Margulies 1998, 1999) resulting in $G'_{axon} = 2190$ Pa and $G''_{axon} = 1793$ Pa at 50 Hz. It is worth noting that the corresponding 'matrix' moduli are $G'_{glia} = 904$ Pa and $G''_{glia} = 372$ Pa, but 'matrix' in Arbogast and Margulies refers to gray matter. Such discrepancies are symptomatic of the general paucity of consistent *in vivo* and *ex vivo* measurements of mechanical properties of human and animal model brains because these properties are regional, depend on method of measurement (frequency and mechanical actuation mode) and adopted mechanical model, and vary with age/post-mortem conditions (Miller *et al* 2000, Miller and Chinzei 2002, Hrapko *et al* 2008, Elkin *et al* 2010, Chatelin *et al* 2010, Shulyakov *et al* 2011, Bilston 2011, Zhang *et al* 2011). Diffusion coefficients for brain white matter were taken from (Sen and Basser 2005).

Homogenization involves the extraction of the effective mechanical properties by averaging the stress-strain relationship over the 2D REV. An explicit description of the viscoelastic and diffusion responses of the tissue in the REV is not feasible as a function of its architecture and the intrinsic material properties of axon, myelin, and glia phases. Nevertheless, a relationship of the following type can be developed numerically

$$\left[G'_{eff}, G''_{eff}, D_{eff} \right] = \mathcal{F}_1 \left(VF_{myelin}, VF_{axon}, G'_p, G''_p, D_p \right). \tag{1}$$

$\mathcal{F}_1$ maps intrinsic properties (subscripted with p) to the effective shear storage modulus G'_{eff} and shear loss modulus G''_{eff} of the tissue REV, and the effective diffusion coefficient D_{eff} as a function of geometrical parameters, such as volume fractions of myelin and axon (VF_{myelin}, VF_{axon}, respectively). The subscript p in the properties appearing in (1) denotes intrinsic (phase-based) values of the viscoelastic moduli in axoplasm (p = axon), myelin sheath (p = myelin), and glial (p = glia) compartments. The complete list of intrinsic properties is: $G'_{axon}, G'_{glia}, G'_{myelin}, G''_{axon}, G''_{glia}, G''_{myelin}, D_{axon}, D_{glia}, D_{myelin}$. Introducing a dimensionless parameter g_{ratio} to describe the myelin thickness, which is defined as the ratio between axon diameter and total fiber diameter, cf figure 1(b), the following relationship holds

$$\frac{VF_{myelin}}{VF_{axon}} = \frac{1 - g_{ratio}^2}{g_{ratio}^2}. \tag{2}$$

In (1), the effective shear storage and shear loss moduli generally depend on the angular frequency ω of the harmonic loading, since the intrinsic properties are also frequency-dependent. By defining a fiber volume fraction $VF = VF_{axon} + VF_{myelin}$, (1–2) can be combined as

$$[G'_{eff}(\omega), G''_{eff}(\omega), D_{eff}] = \mathcal{F}_2 \left(VF, g_{ratio}, G'_p, G''_p, D_p \right). \tag{3}$$

In the following two sections, we demonstrate how the mapping $\mathcal{F}_2$ is computed by developing a mechanical model separately from the diffusion model for the same REV, and then performing sensitivity analysis for a set of inputs given in the RHS of (3).
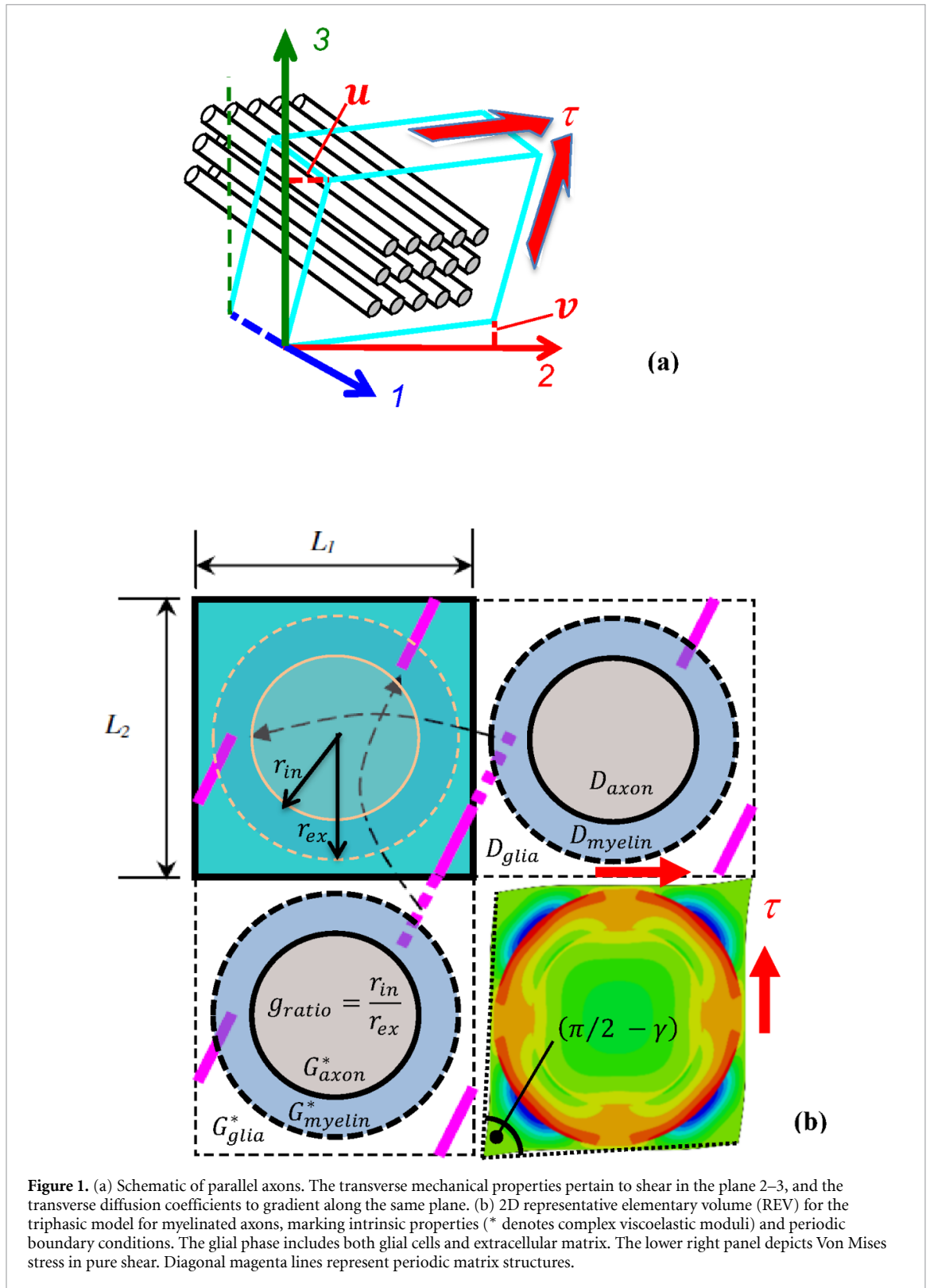
Figure 1. (a) Schematic of parallel axons. The transverse mechanical properties pertain to shear in the plane 2–3, and the transverse diffusion coefficients to gradient along the same plane. (b) 2D representative elementary volume (REV) for the triphasic model for myelinated axons, marking intrinsic properties (* denotes complex viscoelastic moduli) and periodic boundary conditions. The glial phase includes both glial cells and extracellular matrix. The lower right panel depicts Von Mises stress in pure shear. Diagonal magenta lines represent periodic matrix structures.

2.2. Computational mechanical and diffusion models

2.2.1. The mechanical model

The mechanical model is developed by applying a force balance in the triphasic REV considered as a continuum

$$\nabla \cdot \sigma = \rho \frac{\partial^2 \mathbf{u}}{\partial t^2},$$

(4)

where ρ is the density, which is the same in all three phases. $\nabla \cdot \sigma$ denotes the divergence of the (Cauchy) stress σ, and **u** the displacement vector in the REV, both functions of space and time. Given the small strains exhibited in MRE, a linear, isotropic constitutive relationship is considered in each phase between the stress and the strain ε as follows

$$\sigma = \left[\frac{E_p}{3\left(1 - 2\nu_p\right)} - \frac{2G_p}{3} \right] tr\left(\varepsilon\right)\mathbf{I} + 2G_p\varepsilon \; ; \; \varepsilon = \frac{1}{2}\left[\nabla\mathbf{u} + \left(\nabla\mathbf{u}\right)^{\mathbf{T}}\right]. \tag{5}$$

The Young modulus, E_p, shear modulus, G_p, and Poisson ratio, ν_p, represent the piece-wise uniform mechanical properties of each phase, denoted by subscript p, $tr\left(\varepsilon\right)$ is the trace of the strain tensor, and **I** is the second-rank identity tensor.

The triphasic 2D tissue model is subjected to MRE loading conditions, which involves harmonic forcing of the brain at a typical frequency of $f = 50$ Hz. The time dependent response of biological materials to impulse or step functions (Lakes 2009) suggests the suitability of linear viscoelasticity theory for this study. The development of the mechanical model for the white matter involves imposing the value of the average pure shear strain, γ, in the plane 2–3 of the REV (figure 1(a)), and the estimation of the corresponding shear stress τ, cf figure 1(b), i.e. $\sigma_{\mathbf{shear}} = \tau = G_p\gamma$. The validity of the above average constitutive equation has been verified in 3D by imposing a number of forcing scenarios; 3 shearing loads in planes 1–2, 2–3, and 1–3, and 3 tensile loads test in axes 1, 2 and 3. In the following, only the 2–3 plane shear is considered. MRE excitation involves the input of oscillatory shear strain

$$\gamma\left(t\right) = \gamma_0 e^{i\omega t}, \tag{6}$$

where γ_0 is the amplitude of the shear strain, $i = \sqrt{-1}$, and $\omega = 2\pi f$. The engineering shear strain (6) is defined as the sum of the shear components in the plane 2–3 of the strain tensor ε given by (5). The strain experienced at each cycle is $\gamma = 2\varepsilon_{23} = \left(u + v\right)/L$ where u, v are the displacement boundary conditions on the loading planes of the REV, and $L = L_1 = L_2$ is the distance between these planes, cf figure 1(b). At steady state, there is a phase lag ϕ between the shear stress, $\tau\left(t\right)$, and the shear strain, $\gamma\left(t\right)$

$$\tau\left(t\right) = \tau^* e^{i\omega t} = \tau_0 e^{\left(i\omega t + \varphi\right)}, \tag{7}$$

where τ^* is the complex stress amplitude, $\tau^* = \tau_0 e^{i\phi} = \tau_0\left(cos\phi + isin\phi\right)$, and τ_0 is the amplitude of the shear stress. Considering the dynamic relationship between shear stress and strain (4–5), the complex shear moduli of the REV can then be expressed via (6) as

$$\tau\left(t\right) = G_{eff}^*\left(\omega\right)\gamma\left(t\right) = \left[G_{eff}'\left(\omega\right) + iG_{eff}''\left(\omega\right)\right]\gamma_0 e^{i\omega t}. \tag{8}$$

The frequency dependent components of G_{eff}' and G_{eff}'' of (8) are the homogenized (over all three constituent phases in the REV) storage and loss moduli, and can be evaluated using Fourier transforms (FT) in terms of $\tilde{g}\left(\omega\right)$, which is the complex FT of the shear relaxation function $g\left(t\right) = \frac{G_R(t)}{G_\infty} - 1$ (Crawford 1998), as noted below

$$G_{eff}'\left(\omega\right) = G_\infty\left(1 - \omega\Im\left(\tilde{g}\right)\right) \; and \; G_{eff}''\left(\omega\right) = G_\infty\left(\omega\Re\left(\tilde{g}\right)\right). \tag{9}$$

$G_R\left(t\right)$ and G_∞ indicate the time-dependent shear relaxation modulus and the steady state shear modulus, and $\Re\left(\tilde{g}\right), \Im\left(\tilde{g}\right)$ the real and imaginary parts of the complex $\tilde{g}\left(\omega\right)$, respectively. Equation (9) reveals that when a harmonic strain is applied to a viscoelastic material at steady state, the material responds with an in-phase stress of magnitude $G_{eff}'\gamma_0$ (representing the elastic behavior), and an 90° out-of-phase stress magnitude of $G_{eff}''\gamma_0$ (viscous behavior). The phase lag, ϕ, often called loss angle, can finally be expressed as

$$\phi = arctan\left(G_{eff}''\left(\omega\right)/G_{eff}'\left(\omega\right)\right). \tag{10}$$

2.2.2. The diffusion model
The diffusion model is developed here by considering steady-state spin diffusion in the same REV continuum, as defined by (Sen and Basser 2005)

$$0 = \nabla \cdot \left(D_p\nabla C\right), \tag{11}$$

where D_p denotes the diffusion coefficient of spins in phase p, and ∇C is the gradient of the spin concentration. The effective diffusion coefficient (averaged over the REV) is defined by the following equation

$$D_{eff}\overline{\nabla C} = \overline{D_p\nabla C}. \tag{12}$$

The overbar denotes volume averages over the REV, and $\overline{D_p \nabla C}$ is the diffusive spin flux generated from a gradient $\overline{\nabla C}$ along a prescribed direction in a hypothetical diffusion experiment. Here only the transverse diffusion coefficients are considered. Unlike MRE, rather than mimicking the DTI experiment for the definition of effective diffusion coefficient, we adopt the standard definition (12), which is independent of the DTI sequence employed.

2.3. Solution methodology of forward problems

In section 2.2, we have presented the systematic definition of the effective shear moduli G'_{eff} and G''_{eff}, and effective diffusion coefficient D_{eff}, which are based on solving the partial differential equations (4) and (11) (the forward problems). The equations are integrated in 2D and in the REV shown in figure 1(b) containing a triphasic composite, and are supplemented with appropriate periodic boundary conditions on the REV. The inter-phase conditions are continuity of displacement **u** and concentration *C*.

By employing the commercial finite element code ABAQUS, a finite element method was used to integrate the mechanical model and determine the effective viscoelastic properties of an REV of a composite material according to equations (1)–(10), while imposing continuity of displacement **u** at the inter-phase boundaries (phases perfectly joined). This approach has been used extensively for conventional composites (Pan *et al* 2011), and includes both energy and boundary loading methods (Iorga *et al* 2008, Pan *et al* 2008b, a). The axon diameter was fixed at 0.7 μm and the outer bounds of the mechanical model varied depending on the designated volume fraction and g_{ratio}. The domain was meshed with a varying element size of approximately 0.07 μm. The REV was meshed with 8-node biquadratic, reduced integration, hybrid elements and mesh convergence tests were performed, which required ~2000 finite elements. A direct steady-state dynamic solver is used to give the response of the REV under a steady harmonic load of 50 Hz. The load was applied as a displacement boundary condition on the surface nodes, with a harmonic displacement parallel to the face, resulting in a pure shear distortion of the REV, with a shear strain of $\gamma = 0.01$. The faces in the shear plane were assigned a repeated boundary condition, where each node's displacement was matched to a corresponding node on the opposing face, cf figure 1(b). After the steady state harmonic field was computed, the reaction forces necessary to produce the assigned displacements were measured and summed for each face, and the resulting average complex shear stress was found. The effective shear modulus of the REV model was computed based on the pure shear stress loading value and correlated average complex shear strain.

The diffusion model given by equations (11) and (12) was integrated using the analytical solution proposed by (Sen and Basser 2005) for cylindrical axons arranged in a periodic square array. The effective transverse diffusion coefficient given by truncation to 3rd order was used in the present study. The diffusion model is parameterized by cell diameter, g_{ratio}, volume fraction, and diffusion coefficients for the axons, myelin sheath and surrounding glial matrix. Because our results consider only the transverse diffusion coefficient and not the total diffusion tensor trace, the cell diameter does not affect the solution, so it is ignored. Compartmental water concentrations are held constant at $C_{myelin} = 0.50$, $C_{axon} = 0.88$, and $C_{glia} = 0.95$ (Sen and Basser 2005). Transverse diffusion coefficients can be normalized by the glial diffusion coefficient (see equation (12) of Sen and Basser 2005) to provide a non-dimensional relationship between the three diffusion coefficients.

3. Results

Since the analytical solution for the diffusion problem is available in the literature, we comment below only on the validation of the methodology for solving the mechanical problem via ABAQUS. A custom code was written to generate the finite element grid of the REV and to analyze the simulation results, so as to enhance the flexibility of the method for future applications involving more complicated models. The consistency of the numerical solution method was tested by assigning the same value to the viscoelastic properties of all three phases, and then verifying that the resulting effective properties match this value. Next, the numerical solution was compared with analytical expressions, which approximate the effective stiffness properties of unidirectional composites under static loading. These expressions are derived from embedding a single composite cylinder in an equivalent homogeneous medium, resulting in a transversely isotropic material (Christensen 2005). Our results are consistent with the effective transverse shear modulus predictions in Christensen 2005.

3.1. Sensitivity analysis of mechanical model

The purpose of the sensitivity analysis is to study systematically the effect that various intrinsic properties have on the effective properties defined on the REV as per (3). We define here a total of eight variables, which are derived from a combination of the intrinsic material parameters: g_{ratio}, VF, G'_{axon}, G''_{axon}/G'_{axon}, G'_{myelin},

Table 1. Intrinsic mechanical properties and default values of variables. These default ratios and storage moduli correspond to $G''_{axon} = 1804$ Pa, $G''_{myelin} = 2870$ Pa, and $G''_{glia} = 410$ Pa.

Intrinsic material properties	Variables	Default value
Ratio of axon radius to the overall radius of the axon plus myelin sheath thickness	g_{ratio}	0.65
Fiber Volume Fraction	$VF = VF_{axon} + VF_{myelin}$	0.5
Storage modulus of axon	G'_{axon}	2200 Pa
Ratio of the loss modulus to the storage modulus of axon	G''_{axon}/G'_{axon}	0.82
Storage modulus of myelin	G'_{myelin}	3500 Pa
Ratio of the loss modulus to the storage modulus of myelin	G''_{myelin}/G'_{myelin}	0.82
Storage modulus of glia	G'_{glia}	500 Pa
Ratio of the loss modulus to the storage modulus of glia	G''_{glia}/G'_{glia}	0.82
Axon Diameter	$-2r_{in}$	0.70 μm

G''_{myelin}/G'_{myelin}, G'_{glia}, and G''_{glia}/G'_{glia}. These eight variables and their 'default' values can be found in table 1. A decision was made to use the ratios between the storage and loss moduli to define the loss modulus so as to retain the ability to change the elastic modulus of the component material while maintaining a similar viscoelastic behavior. Due to uncertainty in available experimental data, a wide range of the given material properties was used. Based on the literature survey discussed in section 2.1, we consider each phase of the WM as a material with dominant elasticity, i.e. the storage modulus for each phase is higher than its loss modulus. To determine the influence of each independent variable on the resulting effective moduli, several datasets were obtained wherein a single variable was varied while all other variables were held constant. In all mechanical computations, we set the Poisson ratio close to 0.5 ($\nu_p = 0.4995$) to account for the near incompressibility of WM, fix the axon diameter equal to $0.7\,\mu m$, and vary the fiber volume fraction (VF) by varying the overall REV size.

First, we study the influence of each independent variable on the resulting effective moduli Several results are plotted in figures 2(a)–(h), where a single variable is altered while keeping all other variables constant. The effective phase angle ϕ is an additional variable. Figure 2(a) indicates that the effective storage and loss moduli gradually decrease as the g_{ratio} increases. This is because the storage and loss moduli of the myelin are higher than those of the axon, and as implied by equation (4), the ratio VF_{myelin}/VF_{axon} decreases with increasing g_{ratio}. Therefore, as the volume fraction of myelin decreases relative to that of the axon, the effective storage and loss moduli decrease, which means that the homogenized REV tissue appears softer.

Figure 2(b) indicates that the effective storage and loss moduli increase, as the sum $VF_{myelin} + VF_{axon} = VF$ increases. Since axon and myelin have higher storage and loss moduli than the glia matrix, higher volume fractions of axon and myelin result in higher effective moduli. Figure 2(c) shows the effect of the G'_{axon} on the effective moduli while keeping constant $VF = 0.5$ and $g_{ratio} = 0.65$. The first value represents a low volume fraction of the sum of the stiffer phases of axon and myelin, which corresponds to a comparatively large VF_{glia} resulting in low sensitivity of the effective moduli with G'_{axon}. Starting with higher sensitivity to the effective moduli at the lower range of G'_{axon} (<3000 Pa), the sensitivity diminishes at higher values of G'_{axon}. Similar behavior is observed for G'_{myelin}, cf figure 2(e), where the trend is similar to figure 2(c). However, the slope of the G'_{eff} *vs* G'_{myelin} curve is higher than that for the G'_{eff} *vs* G'_{axon} curve, indicating a higher sensitivity of the effective moduli with myelin stiffness. From figures 2(b) and (c) we can deduce that, as the volume fraction of the stiffer phases (axon and myelin) increases, the sensitivity of the effective modulus with respect to G'_{axon} also increases, especially for $VF > 0.5$ where the effective moduli curves is noticeably steeper, see figure 2(b). Regarding the trends of the effective storage and loss moduli with increasing glia stiffness, there are some differences between the results of figure 2(g) and those of figures 2(c) and (e). On one hand, the effective storage and loss moduli should be more sensitive to the intrinsic properties of glia than those for axon or myelin, given the higher glial volume fraction. On the other hand, the glia storage and loss moduli are lower than the intrinsic properties of axon or myelin. As shown in figures 2(c), (e) and (g), the ranges of G'_{glia}, G'_{axon} and G'_{myelin} material properties are disparate: 0–3000 Pa for G'_{glia} and 500–6500 Pa for G'_{axon} and G'_{myelin}. The sharp increase of the effective moduli at low values of G'_{glia} in figure 2(g) indicates the sensitivity of the system to glia properties. At higher G'_{glia} values, the function of G'_{eff} and G''_{eff} *vs* G'_{glia} mimics their variation *vs* G'_{axon} (figure 2(c)), and *vs* G'_{myelin} (figure 2(e)). Taken together, the above observations indicate that *the stiffness of the glial phase is a key influencing parameter to the response of the effective moduli.*

The results of figure 2(d) are based on $G'_{axon} = 2,200 Pa$, and indicate that the ratio G''_{axon}/G'_{axon} affects the effective loss and storage moduli differently. The effective loss modulus increases linearly with G''_{axon}/G'_{axon}. This is consistent with keeping G'_{axon} fixed and assuming a linear viscoelastic constitutive model for the tissue. The effective storage modulus decreases and then asymptotes, which implies that increasing G''_{axon} results in the increase of the effective storage modulus. Similar conclusions can be reached for the effects of
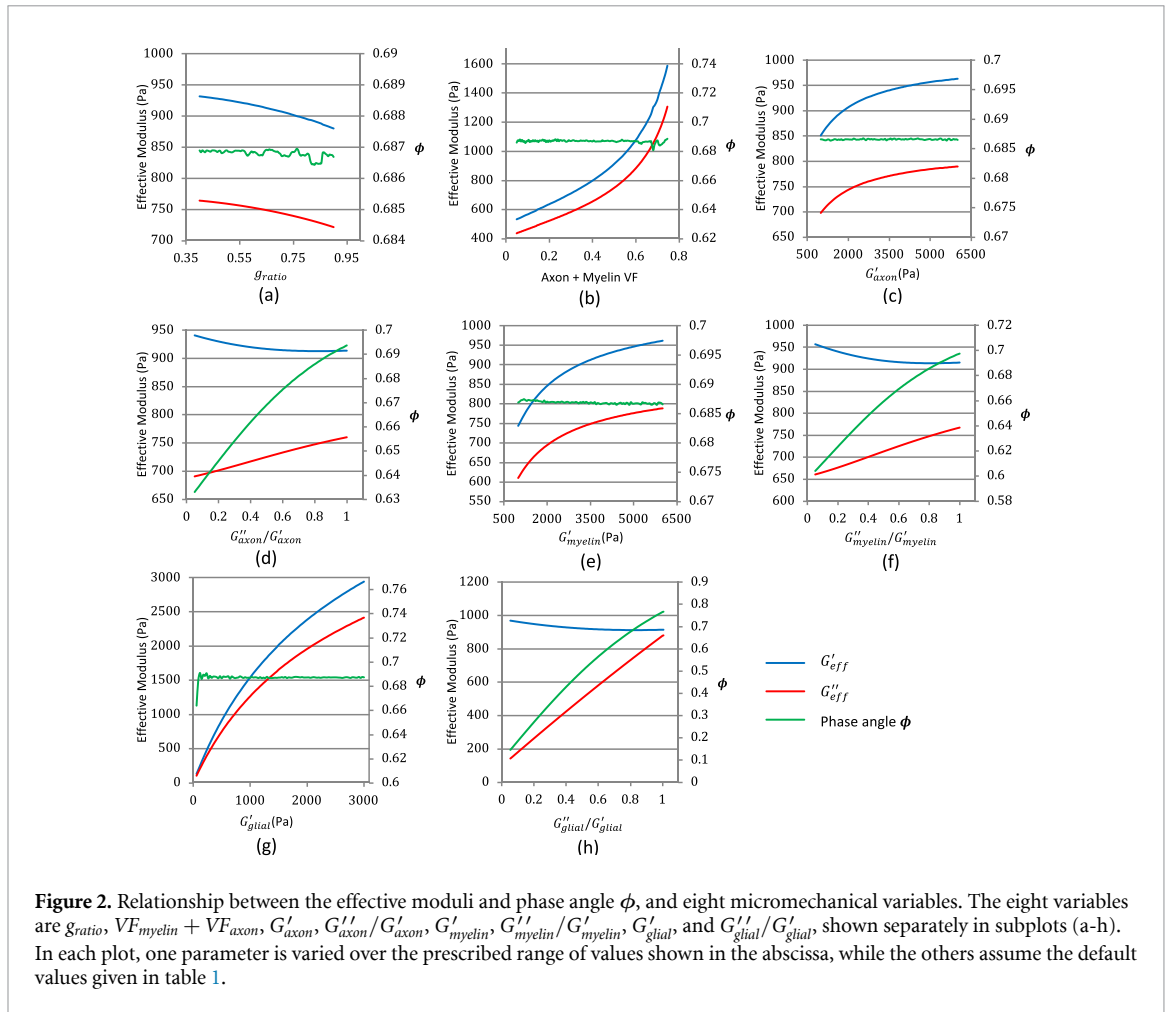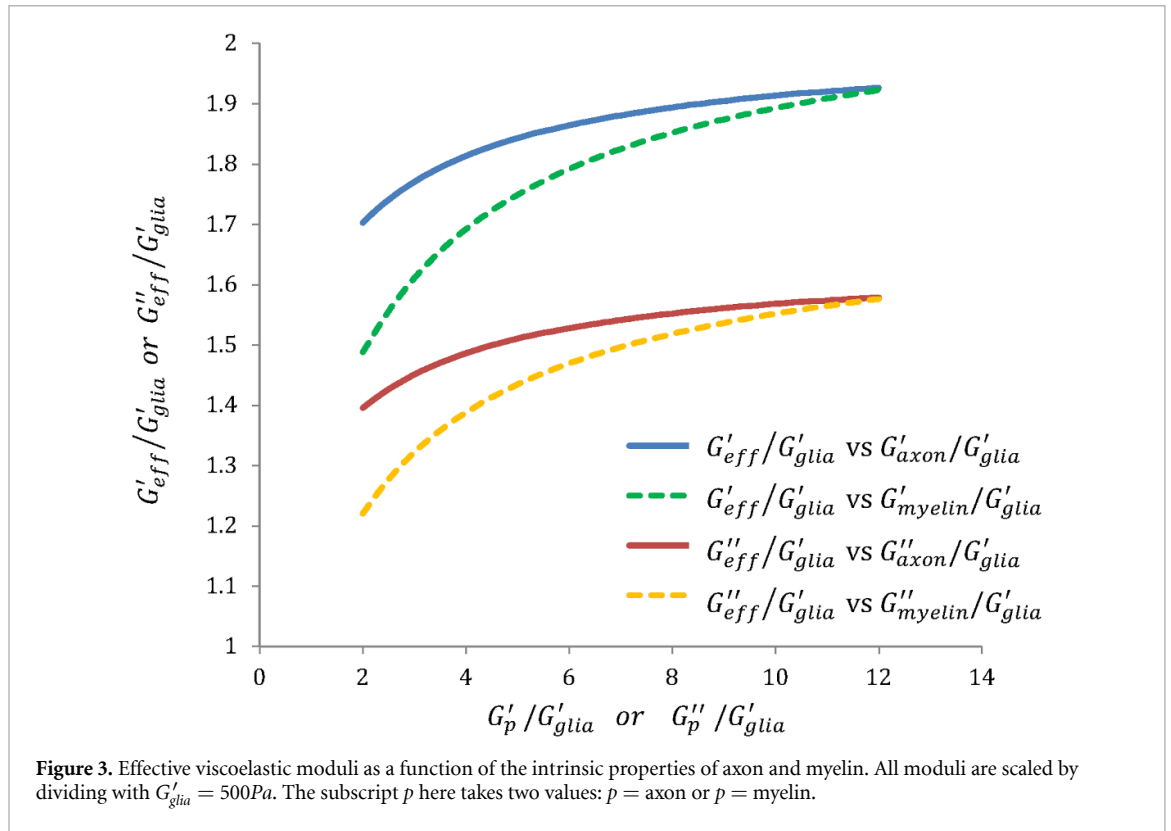
Figure 2. Relationship between the effective moduli and phase angle ϕ, and eight micromechanical variables. The eight variables are g_{ratio}, $VF_{myelin} + VF_{axon}$, G'_{axon}, G''_{axon}/G'_{axon}, G'_{myelin}, G''_{myelin}/G'_{myelin}, G'_{glial}, and G''_{glial}/G'_{glial}, shown separately in subplots (a-h). In each plot, one parameter is varied over the prescribed range of values shown in the abscissa, while the others assume the default values given in table 1.

G''_{myelin} and G''_{glia}, as demonstrated in figures 2(f) and (h). This effect can be shown more clearly by referring to the curves of the phase angle of effective moduli in figures 2(d), (f) and (h). A comparison of these curves indicates that the *largest impact arises from the glia loss modulus*. However, this might be a result of the fact that the glia volume fraction is higher than VF_{myelin} or VF_{axon}.

By inspecting figures 2(a), (b), (c), (e) and (g), the (effective) phase angle ϕ appears relatively insensitive to g_{ratio}, VF, G'_{axon}, G'_{myelin}, and G'_{glia}. On the other hand, the effective loss and storage moduli seem to be very sensitive to the volume fraction VF, G'_{glia}, and G''_{glia}. This is because the glia phase occupies more space than the axon and myelin in the default volume fraction setting ($VF = 0.5$). However, attention should be paid to the effect of the intrinsic properties of axon and myelin. As these moduli increase, their relative contribution to the effective moduli is expected to increase. After setting a constant $G'_{glia} = 500 Pa$, and $VF = 0.5$, the effective moduli are rescaled by dividing with $G'_{glia} = 500 Pa$, and plotted in figure 3 as a function of the intrinsic properties, which are rescaled similarly. The asymptotic convergence of the rescaled intrinsic properties of axon and myelin as their values increase is a manifestation of the fact that the contribution of the glial properties remains dominant for this range. An explanation for this phenomenon can be traced in the way that morphology of the triphasic composite (shown in figure 1(b)) affects the transmission of shear stress across the phases. In 2D, the glia phase is contiguous, while both axon and myelin are non-contiguous. Therefore, it is reasonable to argue that *the contiguous glia phase controls the overall transmission of stress*.

A more systematic sensitivity analysis involves the generation of a large number of quasi-random combinations (samples) of the phase properties, which are input to the ABAQUS simulation package, followed by statistical analysis of the computed effective properties. Six independent variables were considered: the intrinsic storage (G'_p) and loss (G''_p) moduli of each of the three phases ($p = $ glia, $p = $ myelin, $p = $ axon). Using the Sobol sequence (Sobol 2001) to provide uniform coverage of the parameter space while maintaining repeatability, 2500 samples of these variables were generated. In order to only generate samples that relevant to WM tissue properties, certain constraints were imposed. To ensure that the loss modulus is smaller than the corresponding storage modulus for each phase, the intrinsic loss modulus was actually defined by multiplying the storage modulus with a factor between 0.05 and 1. In addition, the glia storage modulus was defined to be categorically smaller than both the axon and myelin storage modulus. By

Figure 3. Effective viscoelastic moduli as a function of the intrinsic properties of axon and myelin. All moduli are scaled by dividing with $G'_{glia} = 500Pa$. The subscript p here takes two values: $p =$ axon or $p =$ myelin.

Table 2. Multiple linear regression analysis of effective storage modulus (VF = 0.26). $R^2 = 0.994$.

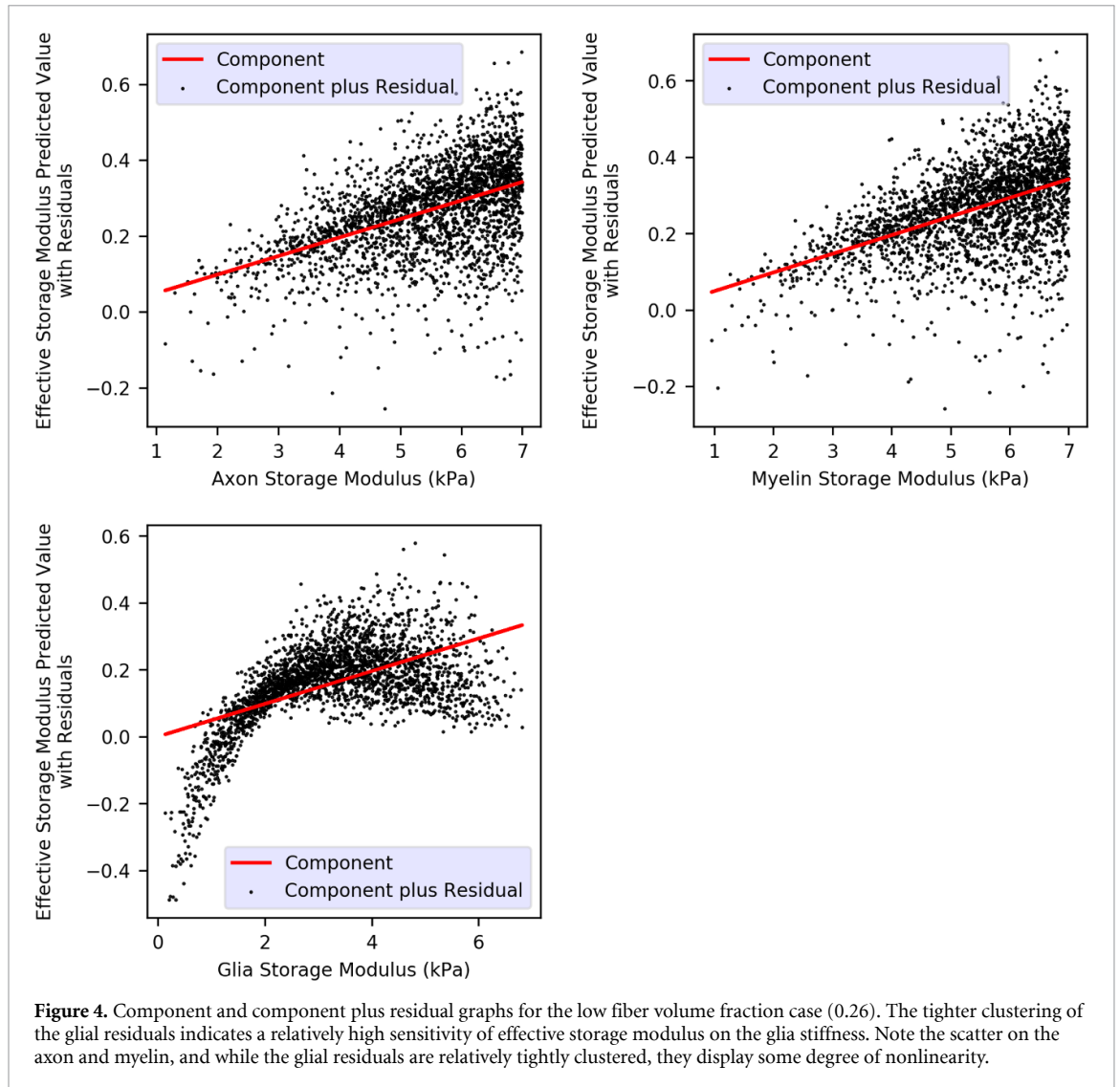|	Coefficient	Standard Error	t	P > |t|	[0.025	0.975]
Constant	−0.0030	0.013	−0.235	0.814	−0.028	0.022
G'_{axon}	0.0489	0.002	25.251	0.0	0.045	0.053
G'_{myelin}	0.0569	0.002	29.900	0.0	0.053	0.061
G'_{glia}	0.9470	0.002	538.633	0.0	0.944	0.950

Table 3. Multiple linear regression analysis of effective storage modulus (VF = 0.74). $R^2 = 0.955$.

	Coefficient	Standard Error	t	P > |t|	[0.025	0.975]
Constant	−0.0916	0.031	−2.998	0.003	−0.151	−0.032
G'_{axon}	0.2054	0.005	44.746	0.0	0.196	0.214
G'_{myelin}	0.3110	0.005	68.886	0.0	0.302	0.320
G'_{glia}	0.5913	0.004	141.856	0.0	0.583	0.599

performing ABAQUS simulations for two fiber volume fractions, $VF = 0.26$ and $VF = 0.74$, and for axon diameter at 0.7 μm and $g_{ratio} = 0.65$, two datasets were then generated, each consisting of 2500 effective moduli. Multiple linear regression analysis using least squares was performed for all independent variables (G'_p and G''_p) on the two datasets. For the regression of G'_{eff} and based on p-values smaller than 0.05, we conclude that only the storage moduli (G'_p) coefficients are non-zero. Therefore, we repeated the regression analysis of G'_{eff} with only G'_p as regressors, and the results are shown in tables 2 and 3 for the two fiber volume fractions.

    In the case of the low $VF = 0.26$ (table 2), the regression results show a significantly higher t-value for the glial storage modulus, indicating a higher sensitivity of the effective properties to glia stiffness. In contrast, although the case of the high $VF = 0.74$ exhibits regression results with higher t-value for the glial storage modulus, the t-values of the glia and the myelin are significantly higher (doubled) than those in the low volume fraction $VF = 0.26$, cf Table 3. Furthermore, the slopes of the component constituents for all axon, myelin, and glial are larger in the 0.74 case than their counterparts in the 0.26 case. While the R^2 values for both fits are quite high, there are some significant outliers, as well as some nonlinearity that cannot be accounted by linear regression analysis. The above analysis highlights the following behaviors: (1) increasing VF increases the system sensitivity to all three phases, and (2) although the effective properties are sensitive
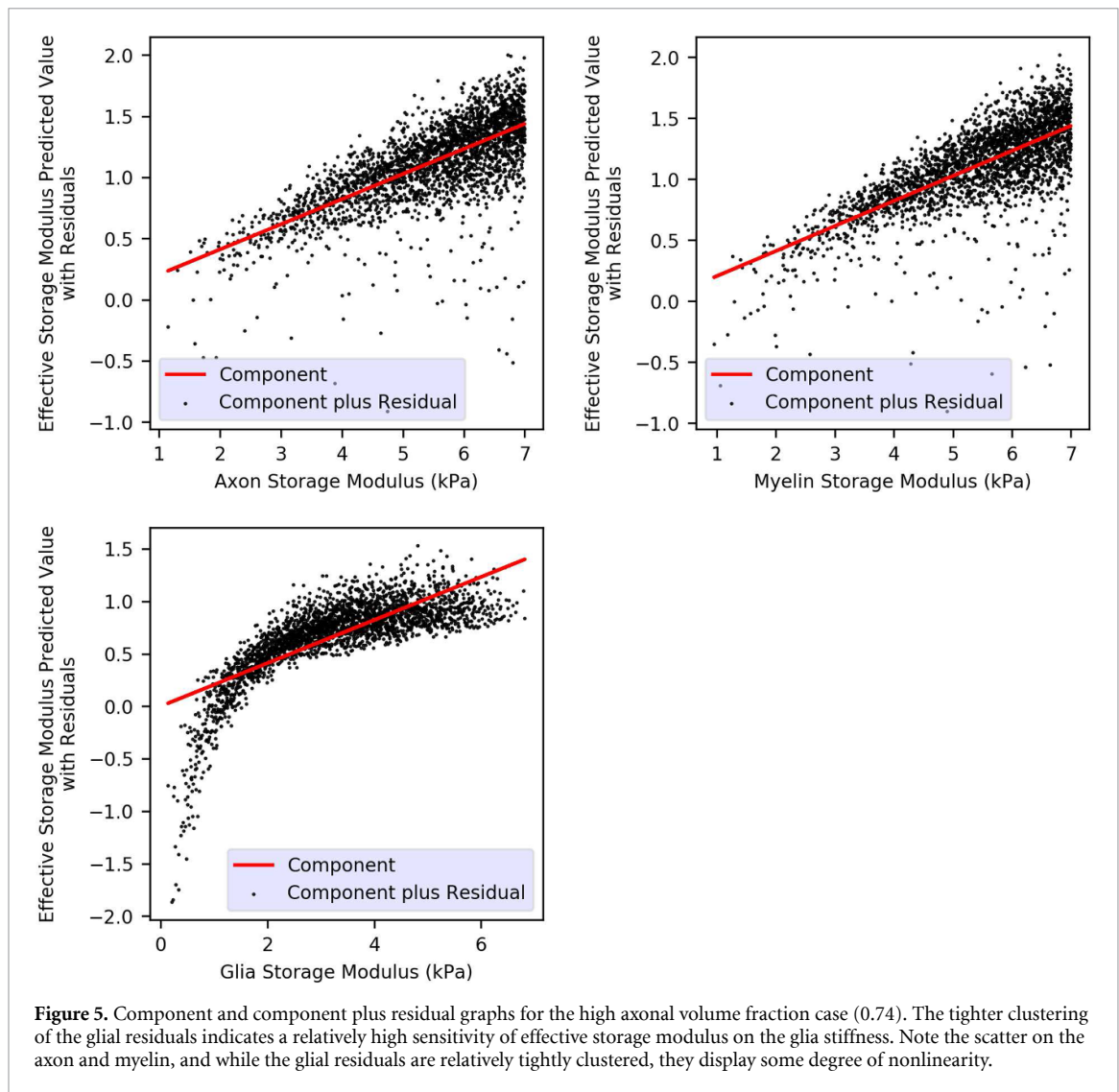
Figure 4. Component and component plus residual graphs for the low fiber volume fraction case (0.26). The tighter clustering of the glial residuals indicates a relatively high sensitivity of effective storage modulus on the glia stiffness. Note the scatter on the axon and myelin, and while the glial residuals are relatively tightly clustered, they display some degree of nonlinearity.

to glia properties for both *VF* values, this sensitivity decreases as *VF* increases from 0.26 to 0.74. This is demonstrated in the component and component plus residual graphs shown in figure 4 for low *VF*, and figure 5 for high *VF*. Note that the glia residuals are relatively tightly clustered around the mean, but there is quite a scatter for the axon and myelin results. Nevertheless, the graphs in figure 5 depict a smaller scatter with larger slopes illustrating the effect of *VF* in our system. The above observations imply that the mapping $\mathcal{F}_2$ in equation (3) is represented by a nonlinear function with respect to *VF*, and suggest that the influence of the glial phase is stronger than that of the axon and the myelin, especially in low *VF*. The above statistical analysis confirms the earlier conclusions made in reference to figures 2 and 3, that *the glial phase is the determining factor of the mechanical response of the WM as a composite.* This deviates from the response of traditional composites where at high VFs the reinforcing phase (here axons) dominates the mechanical behavior. Unlike synthetic (structural) composites, the elastic moduli of the constituents of the brain WM do not exhibit order(s) of magnitude differences. This enhances the effect of the glial response for all volume fractions.

Finally, we observe in figures 4 and 5 an increasing range of residuals with increasing values of the intrinsic moduli for all three phases (axon, myelin, and glia). This increase is a manifestation of the categorical inequalities established between the intrinsic moduli (section 3.1) to represent the observed relationship between the biological properties. As the modulus represented in the abscissa increases in value, so does the range of the other two moduli. This increase in range yields wider range and higher values in the effective modulus, because the latter increases monotonically with the moduli.

3.2. Sensitivity analysis of diffusion model

The parameter ranges chosen for the diffusion model (table 4) match the mechanical model where possible, and also match literature values. A global sensitivity analysis (Saltelli 2002, Saltelli *et al* 2010) of the model

Figure 5. Component and component plus residual graphs for the high axonal volume fraction case (0.74). The tighter clustering of the glial residuals indicates a relatively high sensitivity of effective storage modulus on the glia stiffness. Note the scatter on the axon and myelin, and while the glial residuals are relatively tightly clustered, they display some degree of nonlinearity.

Table 4. Parameter ranges for diffusion problem parameters.

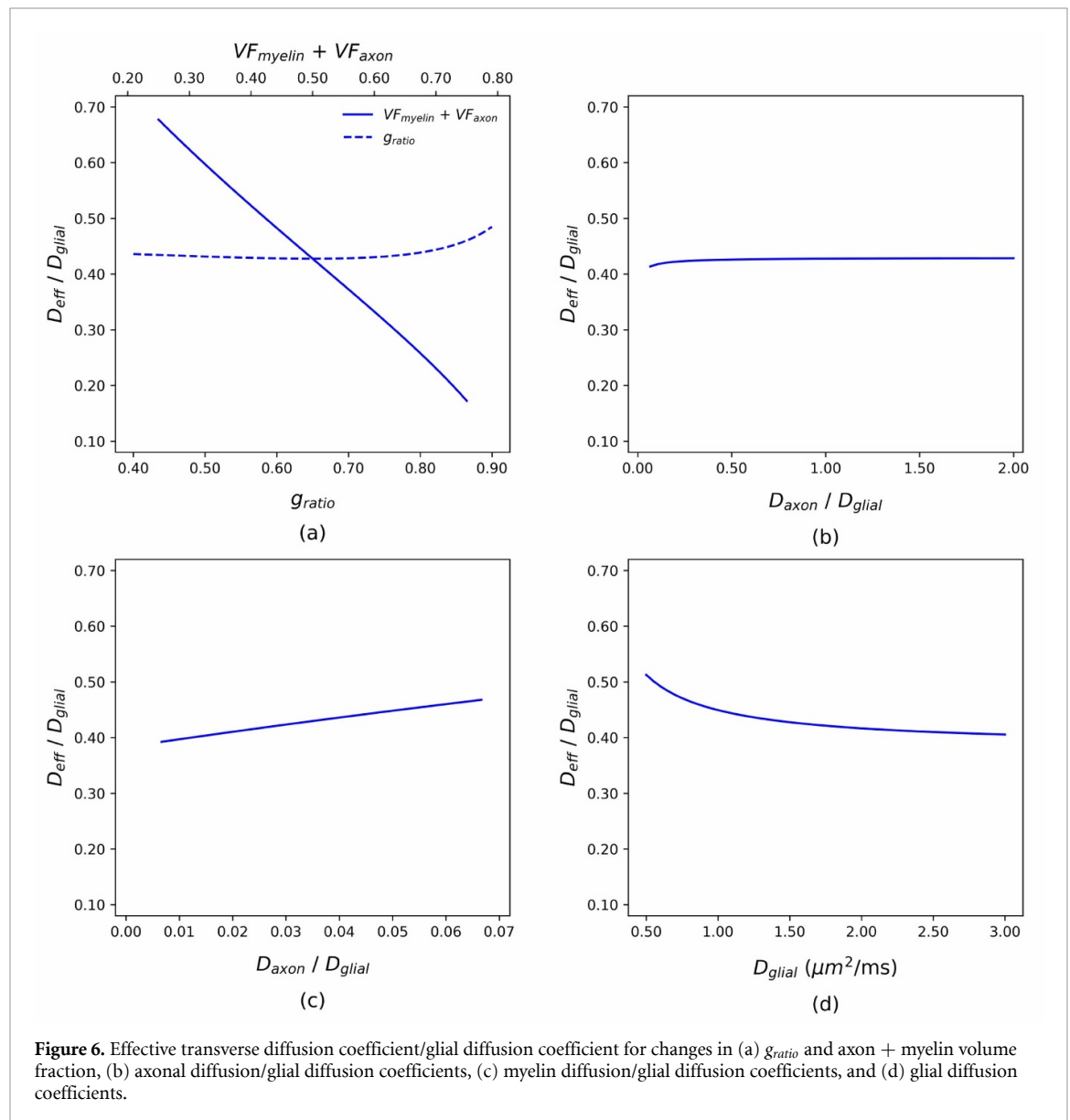| Parameter	Range	Default Value
Axon Diameter	0.40–2.00	0.70 μm
g_{ratio}	0.40–0.90	0.65
$VF_{myelin} + VF_{axon}$	0.25–0.75	0.50
D_{axon}	0.50–3.00	1.50 μm^2/ms
D_{myelin}	0.01–0.10	0.05 μm^2/ms
D_{glia}	0.50–3.00	1.50 μm^2/ms

was preformed using the open source SaLib package in Python (Herman and Usher 2017), which calculates the variance in the output associated with each parameter or combination of parameters. Parameters were sampled with a Sobol sequence (Sobol 2001) with 50 000 samples generated for each parameter, for a total of 700 000 samples. Results are shown in table 5. *Volume fraction (VF) and glia diffusion coefficient (D_{glia}) account for almost all the variance in the transverse effective diffusion coefficient.* This is illustrated in figure 6 where one parameter at a time is varied while all other parameters are held constant. Results are displayed in terms of the effective transverse diffusion coefficient normalized by the glial diffusion coefficient (D_{eff}/D_{glia}) to illustrate that the important relationships in the diffusion model are not the absolute values of the diffusion coefficients but rather the ratios between them. The high sensitivity to changes in volume fraction can be seen in figure 6(a). In fact, the relationship between D_{eff} and volume fraction is quasi-linear and this can be attributed to the barrier action of the myelin sheath. Since the diffusion coefficient of myelin is much lower than that of axon and glia (cf table 4), these two compartments do not exchange many spins during diffusion, so the effective transport coefficient can be approximated by the 'law of mixtures'. The significance

Table 5. Sensitivity indices for diffusion model. Volume fraction ($VF = VF_{myelin} + VF_{axon}$) and glial diffusion ($D_{glia}$) account for 98% of variance in the model.

Parameter	1st Order Indices $\pm$ Confidence Intervals	Total Order Indices $\pm$ Confidence Intervals
g_{ratio}	0.002 ± 0.001	0.005 ± 0.000
VF	0.400 ± 0.008	0.479 ± 0.007
D_{axon}	$< 0.001 \pm 0.000$	$< 0.001 \pm 0.000$
D_{myelin}	0.010 ± 0.001	0.012 ± 0.000
D_{glia}	0.507 ± 0.007	0.586 ± 0.008

	non-zero 2nd Order Indices $\pm$ Confidence Intervals
VF & D_{glia}	0.078 ± 0.014
g_{ratio} & D_{myelin}	0.001 ± 0.001

Figure 6. Effective transverse diffusion coefficient/glial diffusion coefficient for changes in (a) g_{ratio} and axon + myelin volume fraction, (b) axonal diffusion/glial diffusion coefficients, (c) myelin diffusion/glial diffusion coefficients, and (d) glial diffusion coefficients.

of glial diffusion coefficient is shown in figure 6(d). While it may appear that the glial phase does not have as large of an effect as the volume fraction, it is important to remember that all ordinate values are normalized by the glial diffusion coefficient, so the effective diffusion coefficient is, in fact, varying substantially with changes in the glial diffusion coefficient.

4. Discussion

4.1. Choice of triphasic tissue model in REV

Brain WM microstructure revealed through microscopy is indeed very complex (Lee *et al* 2019) so we opted for a canonical REV model to characterize the WM tissue architecture directly. Choosing a simple axonal shape (perfect cylinder) and periodic packing arrangement (square array), simplifying the myelin sheath as a cylindrical annulus, as well as prescribing uniform properties in each phase, is driven by the need to develop an REV that can be related to histology but also described with as few parameters as possible. The first enables the solution of the forward problem for *in silico* MRE and DTI experiments. The second leads to the formulation of tractable inverse problems, i.e. extraction of cell level parameters from the MRE and DTI signal. For DTI, such continuum tissue models allow the interpretation of the signal in terms of biophysical parameters that can be assessed via independent histological assays (Jelescu and Budde 2017, Lee *et al* 2019). However, there is a paucity of systematic computational investigations of the viscoelastic response of such multiphasic systems. The biphasic model in (Arbogast and Margulies 1999) employed approximate expressions for the complex transverse moduli. To our knowledge, the triphasic model presented here is used for the first time to model MRE-relevant harmonic shear stress on the cell level.

Although the assumptions regarding cylinder packing arrangement as well as shear loading direction appear to limit the applicability of the results, these limits are not severe. Prior results for two-phase unidirectional composites (identical parallel cylinders embedded in a homogenous matrix) indicate that the packing arrangement (square vs. hexagonal arrays) does not affect significantly the effective stiffness (Huang *et al* 2008), and the effective diffusivity (Perrins *et al* 1979), for fiber volume fractions of up to 0.6. Similarly, the departure from transverse isotropy is insignificant for effective stiffness (Sertse *et al* 2018), while it is zero for effective diffusivity (Rayleigh 1892), which implies that varying the orientation of the transverse mechanical excitation and diffusion gradient does not affect our results. The last point implies that, as a result of the homogenization over the 2D REV, MRE/DTI models are isotropic with effective properties G'_{eff}, G''_{eff} and D_{eff} *transverse* to WM axons. Since the MRE/DTI metrics along the WM axons are different from the transverse, we conclude that MRE/DTI in 3D should be described by *transversely isotropic* models. Starting with viscoelastic constitutive models for each phase, of course, results in a viscoelastic effective model for the homogenized medium. Finally, there is strong experimental evidence that the brain behaves as a viscoelastic rather than a poroelastic medium at 50 Hz (McGarry *et al* 2015).

Our results presented in sections 3.1 and 3.2 indicate that there exist analogies between effective shear and diffusional properties of the homogenized medium, for example with respect to their sensitivity to the glial phase properties. Nevertheless, there is an important difference in terms of the dependence of effective properties with fiber volume fraction (*VF*). The dependence of effective viscoelastic moduli (G'_{eff}, G''_{eff}) is a nonlinear function of *VF* (cf figure 2(b)), while D_{eff} is an approximately linear function of *VF* (cf figure 6(a)), both for fixed glial properties. The extraction of each effective property involves integration of the governing equation over the REV, but viscoelastic properties constitute a fourth order (elasticity) tensor, while diffusion coefficients form a second order tensor (with eigenvalues given by DTI). The present work indicates that the mechanical problem solution (MRE signal) cannot be approximated by a spatially-weighted superposition of the intrinsic phase contributions, in the same way that the DTI signal is considered as a linear superposition of the various diffusion compartments (Panagiotaki *et al* 2012).

4.2. Importance of model parameters and their combination

The present sensitivity analysis revealed that the effective loss and storage moduli are very sensitive to the fiber volume fraction and the intrinsic loss and storage moduli of the glial phase. On the other hand, the effective phase angle ϕ is insensitive to all parameters other than the ratios G''_{axon}/G'_{axon}, G''_{myelin}/G'_{myelin}, and G''_{glia}/G'_{glia}. Another parameter of interest to brain MRE researchers (Murphy *et al* 2019) is the damping ratio $\xi = \frac{1}{2}tan\phi = \frac{1}{2}G''_{eff}(\omega)/G'_{eff}(\omega)$, which along with the phase angle (10), quantifies the importance of viscous energy dissipated relative to elastic energy stored in the tissue during the shear wave propagation. The above relationship indicates that ξ would be more sensitive than ϕ, as a matter of definition.

Further insight into the sensitivity of the MRE metrics can be obtained by exploiting the non-dimensionalization introduced earlier, whereby all moduli were scaled by dividing with a single intrinsic modulus (G'_{glia}). Since all intrinsic moduli are comparable in magnitude, we can scale them with the same modulus $G'_p \sim G''_p \sim G'_{glia} \sim (10)^3 Pa$, and all length scales with the axon diameter $2r_{in} \sim (10)^{-6}m$. The steady state version of equation (4) yields the following force balance

$$\sum \frac{G'_{glia}}{(2r_{in})^2}||\mathbf{u}|| \sim \rho\omega^2||\mathbf{u}|| \Rightarrow \sum \frac{(10)^3}{(10)^{-12}}||\mathbf{u}|| \sim (10)^3(300)^2||\mathbf{u}||. \tag{13}$$

The Σ operator on the LHS refers to the sum of all the shear stress terms. The above balance implies that the RHS, and therefore the inertia force, is negligible relative to the shear stress in the REV for $f = 50$ Hz. The frequency of harmonic excitation enters in the problem only to the extent that the intrinsic properties of the individual phases depend on frequency (Arbogast and Margulies 1999, Lu *et al* 2006). Based on all the previous discussion regarding similarity laws, the relationship between MRE/DTI metrics and microstructural parameters expressed by the mapping $\mathcal{F}_2$ in (3) can be finally transformed into the following mapping containing only dimensionless parameters

$$\left[\frac{G'_{eff}}{G'_{glia}}, \frac{G''_{eff}}{G'_{glia}}, \frac{D_{eff}}{D_{glia}} \right] = \mathcal{F}_3 \left(VF, g_{ratio}, \frac{G'_{axon}}{G'_{glia}}, \frac{G''_{axon}}{G'_{glia}}, \frac{G'_{myelin}}{G'_{glia}}, \frac{G''_{myelin}}{G'_{glia}}, \frac{D_{axon}}{D_{glia}}, \frac{D_{myelin}}{D_{glia}} \right), \qquad (14)$$

where the frequency dependence of the micromechanical parameters has been suppressed.

Finally, microscopic length scales, such as axon diameter ($2r_{in}$), do not enter in either the steady-state 2D mechanical or the diffusion problem. In our tissue model (3), the effective properties in the transverse plane are only functions of dimensionless geometrical parameters like *VF* and g_{ratio}. Although this conclusion applies directly to MRE, the relationship to DTI metrics is not straightforward because the dMRI signal depends on the specific dMRI sequence employed. Histological analysis indicates that less than 1% of the corpus callosum fibers have diameters larger than $3\mu m$ (Innocenti *et al* 2015). Because the axon diameter is small relative to the spin diffusion radius, the predicted effective radial diffusivity (RD) in WM obtained with realistic clinical dMRI sequences (Sen and Basser Baxter and Frank 2013) is not far from the analytical solution (2005) employed here. This is consistent with the observation that, even with the 300 mT m^{-1} Connectome diffusion gradient, the correlation of RD to axon diameter in the *corpus callosum* remains insignificant (Fan *et al* 2019). We should note in passing that for this high diffusion gradient level, and regardless of the gradient waveform, the theoretical dMRI resolution limit of cylindrical fiber diameter is $2 - 5\mu m$, depending on SNR and fiber orientation dispersion (Nilsson *et al* 2017). Two additional comments are in order regarding the effect of fiber diameter on DTI. First, steady-state DTI metrics do depend on fiber diameter in 3D (Sen and Basser 2005). Second, DTI metrics obtained with finite diffusion time in WM (Lee *et al* 2018) and skeletal muscle (Naughton and Georgiadis 2019a) depend on the fiber diameter. Both these effects can be addressed by extending the present model to 3D and then simulating the DTI signal, as in (Naughton and Georgiadis 2019b).

4.3. Comparisons with MRE and DTI data of brain WM

Rather than further discussing the biophysical (biomechanics and diffusion) aspects of the problem, this section focuses on the import that the presented sensitivity analysis can have on neuroimaging via MRE and DTI. Firstly, no specific MRI sequences or image formation were considered. Secondly, only comparisons with ideal experiments can be made. MRE involves the imposition of oscillatory shear strain followed by the extraction of the effective mechanical properties via the solution of an inverse problem for interpreting the dynamic stress-strain relationship. The proposed model and reported sensitivity analysis results connect the results (effective viscoelastic moduli) of the *perfect* solution of the (anisotropic) inverse problem with white matter microarchitecture and intrinsic properties of the constituents. Similarly, the results of the diffusion study can only be related to DTI studies with short pulse width and long diffusion time limit, where the analytical result of (Sen and Basser 2005) applies (Baxter and Frank 2013). Additionally, our simulations reported here pertain to effective properties in the plane perpendicular to the fiber (plane 2–3 in figure 1(a)), such as the transverse shear moduli and radial diffusion coefficients (RD), although extension to a full 3D study is underway, as discussed in section 4.5 below.

In terms of direct comparisons of the results presented in the previous section with prior data, there exist limited anisotropic MRE and co-registered DTI measurements of brain WM regions. The reason for this paucity is the difficulty of solving the anisotropic inverse problem. (Romano *et al* 2012) introduced an anisotropic inversion method that relies on spatial-spectral filtering of the displacement fields in the corticospinal tracts, and by estimating the storage components of the stiffness tensor, supported the validity of transversely isotropic model for this region in healthy subjects. A follow-up study (Romano *et al* 2014) concluded that, in terms of effective transverse properties, the shear storage modulus (G'_{eff}) decreases and RD $= D_{eff}$ increases significantly in the corticospinal tract of amyotrophic lateral sclerosis (ALS) patients. No loss modulus data were reported. Since ALS is associated with axonal degeneration and consequently decreasing axonal volume fraction (*VF*), the above measurements are consistent with the trends depicted in figures 2(b) and 6(b), if we assume no other parameters change. Two recent anisotropic MRE studies reported that normal aging is associated with the following trends of the effective transverse moduli in the human *corpus callosum*: G'_{eff} decreases (Kalra *et al* 2019), and both G'_{eff}, G''_{eff} decrease with age (Gallo *et al* 2019). Normal aging is correlated with WM demyelination but with stable g_{ratio} (Berman *et al* 2018), hence

both trends contribute to decreasing VF_{myelin} and VF_{axon} according to (2). Both results (Romano *et al* 2014, Gallo *et al* 2019) are thus consistent with the trends depicted in figure 2(b). On the other hand, decreasing $VF_{myelin} + VF_{axon}$ while g_{ratio} is fixed, results in increasing D_{eff} (according to figure 6(b)). This is consistent with the findings of (Hasan *et al* 2009, Bartzokis *et al* 2012) regarding age-related changes in radial diffusivity in the late-myelinating region of human *corpus callosum*, which is composed primarily of small diameter axons.

Incomplete comparisons can be made with an earlier, high resolution study of *in-vivo* brain MRE, albeit one employing an isotropic inversion model (Johnson *et al* 2013a). Two MRE metrics showed high correlation with one DTI metric in the *corpus callosum*: G'_{eff} exhibited positive correlation with RD, and G''_{eff} negative correlation with RD. Given that g_{ratio} varies slowly along the corpus callosum (Berman *et al* 2018), the first trend can be explained by our results in figures 2(b) and 6(b) since $VF_{myelin} + VF_{axon}$ varies strongly along the *corpus callosum* (Björnholm *et al* 2017). The caveat here is that the two measured MRE metrics do not represent only the transverse moduli, but are composite measures of longitudinal and transverse mechanical properties. In addition, there is no evidence that all intrinsic properties (G'_p, G''_p, D_p) remain constant along the *corpus callosum*. We have recently developed an inverse transversely isotropic scheme to extract effective shear viscoelastic properties from multi-excitation MRE, and we employed the extra information provided by the anisotropy of the WM effective properties to estimate the intrinsic properties of axons and glial matrix from a biphasic WM model (Gallo *et al* 2020). Information about the local axon orientation was provided by co-registered DTI data. We confirmed that axons are indeed stiffer than the surrounding glial phase, which is consistent with experiments, and found that intrinsic axonal viscoelastic properties vary along the *corpus callosum* much more widely than that of glia. Although this was based on a biphasic model, this result bolsters our confidence in the integrated MRE-DTI tissue model reported here and motivates future extensions in 3D.

4.4. Limitations of sensitivity indices

In addition to the limitations mentioned above, there are methodological limitations inherent to the sensitivity analysis we employed. Sensitivity indices are only meaningful if the parameter ranges are realistic. These sensitivity indices are global indices and describe the effect over the prescribed range as a whole. The parameter ranges chosen are intentionally broad to include the majority of values reported in the literature. Additional measurements will allow refining these parameter ranges leading to more accurate sensitivity indices. Another limitation of the present DTI study using the periodic unidirectional composite model is that we did not address the effects of WM fiber diameter heterogeneity and orientation dispersion (Veraart *et al* Alexander *et al* 2010, 2019, Lee *et al* 2019), variation of g_{ratio} inside the REV (Lee *et al* 2019), or variable diffusion time (Lee *et al* 2018). Similarly, we have not addressed the effect of variation of the intrinsic mechanical or diffusional properties inside the REV. Finally, we have not assessed the effect of experimental error on the sensitivity relationships in order to determine a minimum SNR level that will allow the correct interpretation of MRE and DTI signals in terms of WM microarchitecture, as was recently demonstrated for skeletal muscle dMRI (Naughton and Georgiadis 2019b). This would require synthesizing the signal from specific MRI sequences for WM as well as describing the solution of the associated inverse problems, which are both outside the scope of this investigation.

4.5. Future and possible extensions

Even in a relatively coherent WM structure, like the *corpus callosum*, there is significant along-axon diameter variation and fiber orientation dispersion (Lee *et al* 2019), so the 2D model needs to be extended. The natural extension of the present methodology is to accommodate 3D brain WM microstructure based on microscopic tissue images. As a next step, 3D REVs will be developed and the homogenization procedures applied here will expand to 3D domains. An assembly of micro-scale 3D REVs will be merged together to construct an integrated macro-scale brain white matter (BWM) finite element model. We will employ assemblies of the homogenized REVs (carriers of material properties and geometric information) to form the elements of the BWM model based on typical fiber volume fractions calculated by the relative distance between the elements and axonal traces. Additional geometric information will be considered in the process of combining the lower level REV model with the higher level model such as the different tortuosity of the axon trace and different volume fractions of the axon. Both of these geometric and material parameters are expected to affect the material properties and thus the response of the brain tissue. More complex, orthotropic or anisotropic material properties will be considered as necessitated by the 3D tissue structure. Each element of the BWM finite element model will be assigned material properties that reflect the information of axon's location and VFs around the axons. The orientation of each BWM element will be based on the information of the orientation of its axonal traces. The above actions will result in a BWM finite element model with both fully defined material properties and material orientation that transcends scales

and will enable the investigation of the dynamic response of brain WM at large scales and under MRE scenarios, while preserving their micromechanical quintessence. Analogous methods will be applied to simulate the DTI signal for brain WM, as was demonstrated in skeletal muscle dMRI (Naughton *et al* 2020).

The presented work is the first step towards developing a realistic 3D simulation framework for performing MRE-DTI *in silico* experiments in complex, histology-based BWM domains (the forward problem). The benefits of this endeavor are multifold. First, this will further inform the selection of the appropriate constitutive model for solving the inverse problem in MRE. Second, this 3D BWM framework will constitute a sophisticated numerical phantom for brain microstructural MRI (Fieremans and Lee 2018). For example, cellular biomechanics can be readily incorporated in our composite model to explore the underlying mechanisms of rapid changes of WM elasticity (Patz *et al* 2019). The high sensitivity of MRE metrics to glial properties reported here might provide useful insights into the observed stiffness variations. Third, it will allow the incorporation of additional WM measurements in addition to MRE/DTI, both *in vivo* and *ex vivo*, towards increasing the specificity of neuroimaging. As an example, the addition of vascular or perivascular spaces to the REV can create improved MRE protocols for the exploration of WM hyperintensities (Gouw *et al* 2008). Fourth, it will enable the integration of new knowledge regarding the mechanical failure of axons (Singh *et al* 2017) in neuroimaging studies of traumatic brain injury (Eierud *et al* 2014).

5. Conclusion

Motivated by the need to interpret the combined measurements of brain MRE and DTI, and to connect MRE metrics (effective shear moduli) to brain white matter (WM) microstructure, we have developed a periodic triphasic tissue model that can accommodate both mechanics and diffusion physics. The model consists of parallel cylindrical inclusions (axons) surrounded by sheaths (myelin), and embedded in a matrix (glial cells plus extracellular matrix). This study focuses on properties defined on the transverse plane, so a two-dimensional REV defined perpendicular to the axons is considered. The mechanical and diffusional properties assigned to each phase are homogeneous and isotropic, consisting of the shear viscoelastic moduli (G'_p, G''_p) and diffusion coefficients (D_p), where $p = axon$, myelin, or glia. Shear deformation is imposed on the REV under harmonic forcing at frequency of $f = 50$ Hz, which is typical of brain MRE, and the effective properties are calculated by solving the motion and diffusion differential equations and averaging over the REV. We concluded that myelinated WM can be appropriately represented by transversely isotropic MRE and DTI constitutive models with metrics (G'_{eff}, G''_{eff}) and D_{eff}, respectively. We then performed a global sensitivity analysis to determine which model parameters are important to the estimated REV-based MRE and DTI metrics. The sensitivity analysis revealed that the effective loss $\left(G'_{eff}\right)$ and storage $\left(G''_{eff}\right)$ moduli are very sensitive to the fiber volume fraction, and the intrinsic storage (G'_{glia}) and loss (G''_{glia}) moduli of the glial phase. On the other hand, the effective phase angle ϕ is insensitive to all parameters other than the ratios G''_{axon}/G'_{axon}, G''_{myelin}/G'_{myelin}, and G''_{glia}/G'_{glia}, and the damping ratio, ξ, is expected to be more sensitive than ϕ, by definition. The effective moduli are nonlinear functions of the fiber volume fraction, as opposed to effective diffusion coefficient, which varies almost linearly. Lastly, the transverse metrics of both MRE and DTI are insensitive to the axon diameter, assuming steady-state excitation, and uniform fiber diameters and parallel fiber arrangement. Based on mathematical arguments, the relationship is expressed in the dimensionless form given by (14).

Our numerical results are consistent with the limited anisotropic MRE and co-registered DTI measurements available in the literature, specifically in the *corpus callosum* and corticospinal tract for normal aging and ALS, respectively. The unidirectional composite model presented here is used for the first time to model the distribution of harmonic shear stress on the cell level under MRE-relevant excitation, and for a wide range of parameters. The unidirectional composite model can be extended to 3D in order to inform the solution of the inverse problem in MRE by establishing which parameters should be included in the model used for inversion. We studied MRE together with DTI because the latter determines the axis of anisotropy for the former, and thus integrating these two modalities ushers in a promise to increase the sensitivity of neuroimaging. Our findings promise to provide useful insights and thus help interpret *in vivo* MRE data. Since the WM model is based on realistic cyto-architectures that can be related to histology, it will also aid in establishing the biological basis of the WM viscoelastic moduli, and integrate MRE/DTI with other modalities towards increasing the specificity of neuroimaging for aging, dementia, or traumatic brain injury studies.

6. Acknowledgments

ORCID iDs

Daniel J Sullivan ● https://orcid.org/0000-0002-3872-7614
Noel M Naughton ● https://orcid.org/0000-0002-5553-4718
John G Georgiadis ● https://orcid.org/0000-0002-8217-2003
Assimina A Pelegri ● https://orcid.org/0000-0003-1145-8175

References

Abolfathi N, Naik A, Chafi M S, Karami G and Ziejewski M 2009 A micromechanical procedure for modelling the anisotropic mechanical properties of brain white matter *Comput. Methods Biomech. Biomed. Eng.* **12** 249–62

Alexander D C, Hubbard P L, Hall M G, Moore E A, Ptito M, Parker G J M and Dyrby T B 2010 Orientationally invariant indices of axon diameter and density from diffusion MRI *Neuroimage* **52** 1374–89

Anderson A T, Van Houten E E, McGarry M D, Paulsen K D, Holtrop J L, Sutton B P, Georgiadis J G and Johnson C L 2016 Observation of direction-dependent mechanical properties in the human brain with multi-excitation MR elastography *J. Mech. Behav. Biomed. Mater.* **59** 538–46

Arani A, Min H-K, Fattahi N, Wetjen N M, Trzasko J D, Manduca A, Jack C R Jr., Lee K H, Ehman R L and Huston J III 2018 Acute pressure changes in the brain are correlated with MR elastography stiffness measurements: initial feasibility in an in vivo large animal model *Magn. Reson. Med.* **79** 1043–51

Arbogast K B and Margulies S S 1998 Material characterization of the brainstem from oscillatory shear tests *J. Biomech.* **31** 801–7

Arbogast K B and Margulies S S 1999 A fiber-reinforced composite model of the viscoelastic behavior of the brainstem in shear *J. Biomech.* **32** 865–70

Assaf Y and Basser P J 2005 Composite hindered and restricted model of diffusion (CHARMED) MR imaging of the human brain *Neuroimage* **27** 48–58

Babaee S, Shahsavari A, Wang P, Picu R and Bertoldi K 2015 Wave propagation in cross-linked random fiber networks *Appl. Phys. Lett.* **107** 211904

Bartzokis G *et al* 2012 Multimodal magnetic resonance imaging assessment of white matter aging trajectories over the lifespan of healthy individuals *Biol. Psychiatry* **72** 1026–34

Baxter G T and Frank L R 2013 A computational model for diffusion weighted imaging of myelinated white matter *Neuroimage* **75** 204–12

Beaulieu C 2009 *Diffusion MRI: From Quantitative Measurement to in Vivo Neuroanatomy* (New York: Academic) pp 105–26

Berman S, West K L, Does M D, Yeatman J D and Mezer A A 2018 Evaluating g-ratio weighted changes in the corpus callosum as a function of age and sex *Neuroimage* **182** 304–13

Bilston L E 2011 *Neural Tissue Biomechanics*, ed L E Bilston (Berlin: Springer)

Björnholm L, Nikkinen J, Kiviniemi V, Nordström T, Niemelä S, Drakesmith M, Evans J, Pike G, Veijola J and Paus T 2017 Structural properties of the human corpus callosum: multimodal assessment and sex differences *Neuroimage* **152** 108–18

Branzoli F, Ercan E, Valabregue R, Wood E T, Buijs M, Webb A and Ronen I 2016 Differentiating between axonal damage and demyelination in healthy aging by combining diffusion-tensor imaging and diffusion-weighted spectroscopy in the human corpus callosum at 7 T *Neurobiol. Aging* **47** 210–7

Chatelin S, Constantinesco A and Willinger R 2010 Fifty years of brain tissue mechanical testing: from in vitro to in vivo investigations *Biorheology* **47** 255–76

Christensen R M 2005 *Mechanics of Composite Materials* (Mineola, NY: Dover Publications)

Crawford R 1998 General properties of plastics *Plastics Engineering* 3rd Edn (*Oxford, UK*: *Elsevier Butterworth-Heinemann*)

De Rooij R, Miller K and Kuhl E 2017 Modeling molecular mechanisms in the axon *Comput. Mech.* **59** 523–37

Dean D C, Hurley S A, Kecskemeti S R, O'grady J P, Canda C, Davenport-Sis N J, Carlsson C M, Zetterberg H, Blennow K and Asthana S 2017 Association of amyloid pathology with myelin alteration in preclinical Alzheimer disease *JAMA Neurol.* **74** 41–49

Duncan G W, Firbank M J, Yarnall A J, Khoo T K, Brooks D J, Barker R A, Burn D J and O'Brien J T 2016 Gray and white matter imaging: A biomarker for cognitive impairment in early Parkinson's disease? *Mov. Disord.* **31** 103–10

Eierud C, Craddock R C, Fletcher S, Aulakh M, King-Casas B, Kuehl D and Laconte S M 2014 Neuroimaging after mild traumatic brain injury: review and meta-analysis *NeuroImage* **4** 283–94

Elkin B S, Ilankovan A and Morrison B 2010 Age-dependent regional mechanical properties of the rat hippocampus and cortex *Trans. ASME, J. Biomech. Eng.* **132** 10

Fan Q, Tian Q, Ohringer N A, Nummenmaa A, Witzel T, Tobyne S M, Klawiter E C, Mekkaoui C, Rosen B R and Wald L L 2019 Age-related alterations in axonal microstructure in the corpus callosum measured by high-gradient diffusion MRI *Neuroimage* **191** 325–36

Feng Y, Okamoto R J, Namani R, Genin G M and Bayly P V 2013 Measurements of mechanical anisotropy in brain tissue and implications for transversely isotropic material models of white matter *J. Mech. Behav. Biomed. Mater.* **23** 117–32

Fern R 2017 The leukocentric theory of neurological disorder: a manifesto *Neurochem. Res.* **42** 2666–72

Fieremans E and Lee -H-H 2018 Physical and numerical phantoms for the validation of brain microstructural MRI: A cookbook *Neuroimage* **182** 39–61

Foerster B R, Welsh R C and Feldman E L 2013 25 years of neuroimaging in amyotrophic lateral sclerosis *Nat. Rev. Neurol.* **9** 513–24

Gallo N R, Cahoon S M, Anderson A T, Naughton N M, Pelegri A A and Georgiadis J G 2020 *ISMRM & SMRT 28th Virtual Conference & Exhibition (8–14 August 2020)* p 0164

Gallo N R, Cahoon S M, Anderson A T, Pelegri A A and Georgiadis J G 2019 *ISMRM 27th Annual Meeting & Exhibition (11–16 May 2019, Montreal, Canada)* p 101

Gatto R G, Chu Y P, Ye A Q, Price S D, Tavassoli E, Buenaventura A, Brady S T, Magin R L, Kordower J H and Morfini G A 2015 Analysis of YFP(J16)-R6/2 reporter mice and postmortem brains reveals early pathology and increased vulnerability of callosal axons in Huntington's disease *Hum. Mol. Genet.* **24** 5285–98

Giordano C and Kleiven S 2014 Connecting fractional anisotropy from medical images with mechanical anisotropy of a hyperviscoelastic fibre-reinforced constitutive model for brain tissue *J. R. Soc. Interface* **11** 20130914

Gouw A A, van der Flier W M, Fazekas F, van Straaten E C, Pantoni L, Poggesi A, Inzitari D, Erkinjuntti T, Wahlund L O and Waldemar G 2008 Progression of white matter hyperintensities and incidence of new lacunes over a 3-year period: the leukoaraiosis and disability study *Stroke* **39** 1414–20

Guerreri M, Palombo M, Caporale A, Fasano F, Macaluso E, Bozzali M and Capuani S 2019 Age-related microstructural and physiological changes in normal brain measured by MRI γ-metrics derived from anomalous diffusion signal representation *Neuroimage* **188** 654–67

Guertler C A, Okamoto R J, Schmidt J L, Badachhape A A, Johnson C L and Bayly P V 2018 Mechanical properties of porcine brain tissue in vivo and ex vivo estimated by MR elastography *J. Biomech.* **69** 10–18

Guo J, Posnansky O, Hirsch S, Scheel M, Taupitz M, Braun J and Sack I 2012 Fractal network dimension and viscoelastic powerlaw behavior: II. an experimental study of structure-mimicking phantoms by magnetic resonance elastography *Phys. Med. Biol.* **57** 4041–53

Hall M G and Alexander D C 2009 Convergence and parameter choice for Monte-Carlo simulations of diffusion MRI *IEEE Trans. Med. Imaging* **28** 1354–64

Hasan K M, Kamali A, Iftikhar A, Kramer L A, Papanicolaou A C, Fletcher J M and Ewing-Cobbs L 2009 Diffusion tensor tractography quantification of the human corpus callosum fiber pathways across the lifespan *Brain Res.* **1249** 91–100

Herman J and Usher W 2017 Salib: an open-source python library for sensitivity analysis *J. Open Source Software* **2** 97

Hrapko M, van Dommelen J A W, Peters G W M and Wismans J 2008 The influence of test conditions on characterization of the mechanical properties of brain tissue *Trans. ASME, J. Biomech. Eng.* **130** 10

Huang Y C, Jin K K and Ha S K 2008 Effects of fiber arrangement on mechanical behavior of unidirectional composites *J. Compos. Mater.* **42** 1851–71

Innocenti G M, Caminiti R and Aboitiz F 2015 Comments on the paper by Horowitz et al. (2014) *Brain Struct. Funct.* **220** 1789–90

Iorga L, Pan Y and Pelegri A 2008 Numerical characterization of material elastic properties for random fiber composites *J. Mech. Mater. Struct.* **3** 1279–98

Jelescu I O and Budde M D 2017 Design and validation of diffusion MRI models of white matter *Front. Phys.* **5** 61

Johnson C L, Holtrop J L, Mcgarry M D J, Weaver J B, Paulsen K D, Georgiadis J G and Sutton B P 2014 3D multislab, multishot acquisition for fast, whole-brain MR elastography with high signal-to-noise efficiency *Magn. Reson. Med.* **71** 477–85

Johnson C L, Mcgarry M D J, Gharibans A A, Weaver J B, Paulsen K D, Wang H, Olivero W C, Sutton B P and Georgiadis J G 2013a Local mechanical properties of white matter structures in the human brain *Neuroimage* **79** 145–52

Johnson C L, Mcgarry M D J, Van Houten E E W, Weaver J B, Paulsen K D, Sutton B P and Georgiadis J G 2013b Magnetic resonance elastography of the brain using multishot spiral readouts with self-navigated motion correction *Magn. Reson. Med.* **70** 404–12

Kaden E, Kruggel F and Alexander D C 2016 Quantitative mapping of the per-axon diffusion coefficients in brain white matter *Magn. Reson. Med.* **75** 1752–63

Kalra P, Raterman B, Mo X and Kolipaka A 2019 Magnetic resonance elastography of brain: comparison between anisotropic and isotropic stiffness and its correlation to age *Magn. Reson. Med.* **82** 671–9

Kiselev V G 2017 Fundamentals of diffusion MRI physics *NMR Biomed.* **30** e3602

Lakes R 2009 *Viscoelastic Materials* (Cambridge: Cambridge University Press) (https://doi.org/10.4236/wjm.2011.13021 9,703)

Le Bihan D and Johansen-Berg H 2012 Diffusion MRI at 25: exploring brain tissue structure and function *Neuroimage* **61** 324–41

Lee -H-H, Fieremans E and Novikov D S 2018 What dominates the time dependence of diffusion transverse to axons: intra-or extra-axonal water? *Neuroimage* **182** 500–10

Lee -H-H, Yaros K, Veraart J, Pathan J L, Liang F-X, Kim S G, Novikov D S and Fieremans E 2019 Along-axon diameter variation and axonal orientation dispersion revealed with 3D electron microscopy: implications for quantifying brain white matter microstructure with histology and diffusion MRI *Brain Struct. Funct.* **224** 1469–88

Liu Y-L, Li G-Y, He P, Mao Z-Q and Cao Y 2017 Temperature-dependent elastic properties of brain tissues measured with the shear wave elastography method *J. Mech. Behav. Biomed. Mater.* **65** 652–6

Liu Y-L, Liu D, Xu L, Su C, Li G-Y, Qian L-X and Cao Y 2018 In vivo and ex vivo elastic properties of brain tissues measured with ultrasound elastography *J. Mech. Behav. Biomed. Mater.* **83** 120–5

Lu Y B *et al* 2006 Viscoelastic properties of individual glial cells and neurons in the CNS *Proc. Natl Acad. Sci. USA* **103** 17759–64

McGarry M, Johnson C, Sutton B, Georgiadis J, Van Houten E, Pattison A, Weaver J and Paulsen K 2015 Suitability of poroelastic and viscoelastic mechanical models for high and low frequency MR elastography *Med. Phys.* **42** 947–57

McGarry M D J, Johnson C L, Sutton B P, Georgiadis J G, Van Houten E, Weaver J B and Paulsen K D 2013 Including spatial information in nonlinear inversion MR elastography using soft prior regularization *IEEE Trans. Med. Imaging* **32** 1901–9

McGarry M D J, Van Houten E, Johnson C L, Georgiadis J G, Sutton B P, Weaver J B and Paulsen K D 2012 Multi-resolution MR elastography using non-linear inversion *Med. Phys.* **39** 6388–96

Miller K and Chinzei K 2002 Mechanical properties of brain tissue in tension *J. Biomech.* **35** 483–90

Miller K, Chinzei K, Orssengo G and Bednarz P 2000 Mechanical properties of brain tissue in-vivo: experiment and computer simulation *J. Biomech.* **33** 1369–76

Morrison J H and Hof P R 1997 Life and death of neurons in the aging brain *Science* **278** 412–9

Murphy M C, Huston J and Ehman R L 2019 MR elastography of the brain and its application in neurological diseases *Neuroimage* **187** 176–83

Muthupillai R, Lomas D J, Rossman P J, Greenleaf J F, Manduca A and Ehman R L 1995 Magnetic resonance elastography by direct visualization of propagating acoustic strain waves *Science* **269** 1854–7

Naughton N M and Georgiadis J G 2019a Comparison of two-compartment exchange and continuum models of dMRI in skeletal muscle *Phys. Med. Biol.* **64** 155004

Naughton N M and Georgiadis J G 2019b Global sensitivity analysis of skeletal muscle dMRI metrics: effects of microstructural and pulse parameters *Magn. Reson. Med.* **83** 1458–70

Naughton N M, Tennyson C G and Georgiadis J G 2020 Lattice Boltzmann method for simulation of diffusion magnetic resonance imaging physics in multiphase tissue models *Phys. Rev. E* **102** 043305

Nilsson M, Lasic S, Drobnjak I, Topgaard D and Westin C F 2017 Resolution limit of cylinder diameter estimation by diffusion MRI: the impact of gradient waveform and orientation dispersion *NMR Biomed.* **30**

Pan Y, Iorga L and Pelegri A A 2008a Analysis of 3D random chopped fiber reinforced composites using FEM and random sequential adsorption *Comput. Mater. Sci.* **43** 450–61

Pan Y, Iorga L and Pelegri A A 2008b Numerical generation of a random chopped fiber composite RVE and its elastic properties *Compos. Sci. Technol.* **68** 2792–8

Pan Y, Shreiber D I and Pelegri A A 2011 A transition model for finite element simulation of kinematics of central nervous system white matter *IEEE Trans. Biomed. Eng.* **58** 3443–6

Pan Y, Shreiber D I and Pelegri A A 2020 On the transversely isotropic, hyperelastic response of CNS white matter using a hybrid approach *ASME J. Med. Diagn.* **4** 011005

Pan Y, Sullivan D, Shreiber D I and Pelegri A A 2013 Finite element modeling of CNS white matter kinematics: use of a 3D RVE to determine material properties *Front. Bioeng. Biotechnol.* **1** 19

Panagiotaki E, Schneider T, Siow B, Hall M G, Lythgoe M F and Alexander D C 2012 Compartment models of the diffusion MR signal in brain white matter: A taxonomy and comparison *Neuroimage* **59** 2241–54

Papazoglou S, Rump J, Braun J and Sack I 2006 Shear wave group velocity inversion in MR elastography of human skeletal muscle *Magn. Reson. Med.* **56** 489–97

Patz S, Fovargue D, Schregel K, Nazari N, Palotai M, Barbone P E, Fabry B, Hammers A, Holm S and Kozerke S 2019 Imaging localized neuronal activity at fast time scales through biomechanics *Sci. Adv.* **5** eaav3816

Perrins W T, Mckenzie D R and Mcphedran R C 1979 Transport properties of regular arrays of cylinders *Proc. R. Soc.* A **369** 207–25

Posnansky O, Guo J, Hirsch S, Papazoglou S, Braun J and Sack I 2012 Fractal network dimension and viscoelastic powerlaw behavior: I. A modeling approach based on a coarse-graining procedure combined with shear oscillatory rheometry *Phys. Med. Biol.* **57** 4023–40

Qin E C, Sinkus R, Geng G, Cheng S, Green M, Rae C D and Bilston L E 2013 Combining MR elastography and diffusion tensor imaging for the assessment of anisotropic mechanical properties: a phantom study *J. Magn. Reson. Imaging* **37** 217–26

Rayleigh L 1892 LVI. On the influence of obstacles arranged in rectangular order upon the properties of a medium *London Edinburgh Dublin Philos. Mag. J. Sci.* **34** 481–502

Recchia S, Zheng J and Pelegri A A 2014 Fiberwalk: a random walk approach to fiber representative volume element creation *Acta Mech.* **225** 1301–12

Romano A, Guo J, Prokscha T, Meyer T, Hirsch S, Braun J, Sack I and Scheel M 2014 In vivo waveguide elastography: effects of neurodegeneration in patients with amyotrophic lateral sclerosis *Magn. Reson. Med.* **72** 1755–61

Romano A, Scheel M, Hirsch S, Braun J and Sack I 2012 In vivo waveguide elastography of white matter tracts in the human brain *Magn. Reson. Med.* **68** 1410–22

Ruoslahti E 1996 Brain extracellular matrix *Glycobiology* **6** 489–92

Saab A S and Nave K A 2017 Myelin dynamics: protecting and shaping neuronal functions *Curr. Opin. Neurobiol.* **47** 104–12

Saltelli A 2002 Making best use of model evaluations to compute sensitivity indices *Comput. Phys. Commun.* **145** 280–97

Saltelli A, Annoni P, Azzini I, Campolongo F, Ratto M and Tarantola S 2010 Variance based sensitivity analysis of model output. design and estimator for the total sensitivity index *Comput. Phys. Commun.* **181** 259–70

Schiessel H and Blumen A 1995 Mesoscopic pictures of the sol-gel transition - ladder models and fractal networks *Macromolecules* **28** 4013–9

Schmidt J, Tweten D, Benegal A, Walker C, Portnoi T, Okamoto R, Garbow J and Bayly P 2016 Magnetic resonance elastography of slow and fast shear waves illuminates differences in shear and tensile moduli in anisotropic tissue *J. Biomech.* **49** 1042–9

Schmidt J L, Tweten D J, Badachhape A A, Reitera A J, Okamoto R J, Garbow J R and Bayly P V 2018 Measurement of anisotropic mechanical properties in porcine brain white matter ex vivo using magnetic resonance elastography *J. Mech. Behav. Biomed. Mater.* **79** 30–37

Sen P N and Basser P J 2005 A model for diffusion in white matter in the brain *Biophys. J.* **89** 2927–38

Sertse H M, Goodsell J, Ritchey A J, Pipes R B and Yu W B 2018 Challenge problems for the benchmarking of micromechanics analysis: level I initial results *J. Compos. Mater.* **52** 61–80

Shreiber D I, Hao H L and Elias R A I 2009 Probing the influence of myelin and glia on the tensile properties of the spinal cord *Biomech. Model. Mechanobiol.* **8** 311–21

Shulyakov A V, Cenkowski S S, Buist R J and Del Bigio M R 2011 Age-dependence of intracranial viscoelastic properties in living rats *J. Mech. Behav. Biomed. Mater.* **4** 484–97

Singh S, Pelegri A A and Shreiber D I 2017 Estimating axonal strain and failure following white matter stretch using contactin-associated protein as a fiduciary marker *J. Biomech.* **51** 32–41

Sinkus R, Tanter M, Catheline S, Lorenzen J, Kuhl C, Sondermann E and Fink M 2005a Imaging anisotropic and viscous properties of breast tissue by magnetic resonance-elastography *Magn. Reson. Med.* **53** 372–87

Sinkus R, Tanter M, Xydeas T, Catheline S, Bercoff J and Fink M 2005b Viscoelastic shear properties of in vivo breast lesions measured by MR elastography *Magn. Reson. Imaging* **23** 159–65

Sobol I M 2001 Global sensitivity indices for nonlinear mathematical models and their Monte Carlo estimates *Math. Comput. Simul.* **55** 271–80

Song S K, Yoshino J, Le T Q, Lin S J, Sun S W, Cross A H and Armstrong R C 2005 Demyelination increases radial diffusivity in corpus callosum of mouse brain *Neuroimage* **26** 132–40

Stanisz G J, Szafer A, Abd R M and Henkelman G A W 1997 An analytical model of restricted diffusion in bovine optic nerve *Magn. Reson. Med.* **37** 103–11

Stikov N *et al* 2015 In vivo histology of the myelin g-ratio with magnetic resonance imaging *Neuroimage* **118** 397–405

Sullivan E V, Rohlfling T and Pfefferbaum A 2010 Quantitative fiber tracking of lateral and interhemispheric white matter systems in normal aging: relations to timed performance *Neurobiol. Aging* **31** 464–81

Sun S W, Liang H F, Trinkaus K, Cross A H, Armstrong R C and Song S K 2006 Noninvasive detection of cuprizone induced axonal damage and demyelination in the mouse corpus callosum *Magn. Reson. Med.* **55** 302–8

Tzschätzsch H, Kreft B, Schrank F, Bergs J, Braun J and Sack I 2018 In vivo time-harmonic ultrasound elastography of the human brain detects acute cerebral stiffness changes induced by intracranial pressure variations *Sci. Rep.* **8** 17888

Velardi F, Fraternali F and Angelillo M 2006 Anisotropic constitutive equations and experimental tensile behavior of brain tissue *Biomech. Model. Mechanobiol.* **5** 53–61

Veraart J, Fieremans E and Novikov D S 2019 On the scaling behavior of water diffusion in human brain white matter *Neuroimage* **185** 379–87

Wang Y *et al* 2011 Quantification of increased cellularity during inflammatory demyelination *Brain* **134** 3587–98

West K L, Kelm N D, Carson R P, Gochberg D F, Ess K C and Does M D 2018 Myelin volume fraction imaging with MRI *Neuroimage* **182** 511–21

Wu X, Georgiadis J and Pelegri A A 2019 Brain white matter model of orthotropic viscoelastic properties in frequency domain *ASME 2019 Int. Mech. Eng. Congress and Exposition (11–14 November 2019, Salt Lake City, UT)* p V003T04A024

Yousefsani S A, Shamloo A and Farahmand F 2018 Micromechanics of brain white matter tissue: A fiber-reinforced hyperelastic model using embedded element technique *J. Mech. Behav. Biomed. Mater.* **80** 194–202

Zhang J, Green M A, Sinkus R and Bilston L E 2011 Viscoelastic properties of human cerebellum using magnetic resonance elastography *J. Biomech.* **44** 1909–13

Zhao X and Pelegri A A 2014a Dynamic simulation of viscoelastic soft tissue in acoustic radiation force creep imaging *J. Biomech. Eng.* **136** 094502

Zhao X and Pelegri A A 2014b Modelling of global boundary effects on harmonic motion imaging of soft tissues *Comput. Methods Biomech. Biomed. Eng.* **17** 1021–31

Zhao X and Pelegri A A 2016 A Bayesian approach for characterization of soft tissue viscoelasticity in acoustic radiation force imaging *Int. J. Numer. Methods Biomed.* **32** e02741